1507

Microfabrication of combined Scanning Near-field Optical and Scanning Force Microscopy probes

A dissertation submitted to the Faculty of Sciences of the University of Neuchâtel, in fulfillment of the requirements for the degree of "Docteur ès Sciences"

by

Gregor Schürmann

Diplômé en électronique-physique de l'Université de Neuchâtel

Institute of Microtechnology
University of Neuchâtel
Rue Jacquet-Droz 1, CH-2007 Neuchâtel
Switzerland

2000

IMPRIMATUR POUR LA THÈSE

Microfabrication of combined Scanning Near-field Optical and Scanning Force Microscopy probes

de M. Gregor Schürmann

UNIVERSITÉ DE NEUCHÂTEL

FACULTÉ DES SCIENCES

La Faculté des sciences de l'Université de Neuchâtel sur le rapport des membres du jury,

MM. N. de Rooij (directeur de thèse), H.P. Herzig, U. Stauffer, A.J. Meixner (Siegen D) et H. Heinzelmann (CSEM)

autorise l'impression de la présente thèse.

Neuchâtel, le 29 mai 2000

Le doyen:

J.-P. Derendinger

Table of contents

1 Introduction

Standard optical microscopy is the most widely used tool for the observation of objects. It is very appreciated because it allows seeing into volumes, is noninvasive, fast, and has many different contrast mechanisms such as intensity, color, polarization and phase. All these signals give different information about the nature of the sample. Unfortunately the resolution of these microscopes is limited by diffraction to around half a micron for visible light [1]. More complicated confocal microscopes, which illuminate the sample locally instead of globally, achieve a resolution of 0.2 microns [2]. In some particular application fields, however, this resolution is not enough. These limitations have triggered the development of Scanning Near-field Optical Microscopy (SNOM) which can generate optical as well as topographical images of a sample surface with a lateral resolution in the nanometer range. An important application field of SNOM is the observation of biological samples such as stained tissue sections and living cells. Furthermore special fluorescent-labeled molecules and the local magnetic properties of thin-films can be studied. SNOM also plays a role in high-density optical data storage where the reading and writing of nanometer sized structures is required. An overview of the current development state of SNOM and its application fields can be found in [3].

Like all other scanning probe microscopy (SPM) methods, SNOM relies on a miniaturized probe scanned across the surface of the sample within very close distance to it. At each point on the sample a certain physical signal is measured, and finally the image is reconstructed in a computer point by point. For example a Scanning Force Microscope (SFM) or

Atomic Force Microscope (AFM) uses a sharp tip at the end of a soft cantilever to probe the surface. The forces acting between the tip apex and the sample surface are detected by measuring the deflection of the cantilever. In the case of SNOM, the signals of interest are the local optical intensity, phase and polarization. As in all other scanning probe techniques, SNOM requires an extremely precise control of the distance between the probe and the sample surface. The aim being to keep the distance between the probe and the sample constant and small enough (keep the probe in the near field) so that the measured optical field has not propagated and no information is lost through diffraction. This distance regulation is made using another near field effect, like for example inter-atomic forces or tunneling currents.

A SNOM tip usually consists of a transparent tip covered with an opaque metal layer into which an aperture is machined at the apex. The tip is scanned over the sample and the light transmitted through the aperture is detected. The resolution of the SNOM is largely determined by the diameter of this aperture. The idea of the aperture SNOM was already proposed in 1928 by Synge [4], but not until the early 1980's was it first technically realized by Pohl et al. and Dürig et al. [5].
Most SNOM microscopes use specially processed optical fibers as probes. The end of these fibers is formed into a tip either by simultaneous heating and pulling or by a special etching process [6,7]. Then the aperture is created by evaporating metal onto the tip at an angle such that the tip apex is not covered [7]. Other processes exist where the fiber is totally covered with metal and the aperture is formed by locally removing it at the tip apex, using an etching agent [8,9] or a Focused Ion Beam (FIB) [10,11,12]. A drawback of these fabrication processes is they do not allow for a great number of probes to be fabricated simultaneously. Furthermore

the probes do not have reproducible properties and are delicate to handle because of their fragility.

In most cases the distance control between the fiber-tip and the sample is achieved with the so-called shear force detection scheme. In this method, the fiber is placed vertically over the sample and oscillated laterally at its resonance frequency. Different forces dampen this oscillation when the tip apex of the fiber gets close to the surface. The dampening is used as a feedback signal to control the distance very accurately. Because of this configuration the probes are very stiff in the direction perpendicular to the sample surface which in turn makes them prone to damage during scanning. All these small disadvantages make actual SNOM microscopes quite difficult to use.

For these different reasons SNOM microscopy is not yet a widely used tool for characterizing surfaces and its use is still limited to specialists.

One very promising way of getting past some of these disadvantages is to build the SNOM sensor using well-established microfabrication techniques. Microfabrication was the key for the breakthrough of Scanning Force Microscopy and routinely enables AFM probes to be batch fabricated in great numbers [13]. The present thesis is motivated by the fact that this technology also has the potential of mass-producing SNOM probes in a reproducible way. Furthermore, microfabrication techniques allow the integration of the SNOM tip on an AFM cantilever. Such combined SFM and SNOM sensors make it possible to benefit from the precision and ease of use of an AFM microscope, with the added information of SNOM.

The work of this thesis deals with the fabrication of combined SFM and SNOM sensors. The aim is to use microfabrication technology to produce new probes with improved characteristics.

1.1 References

[1] E. Abbe, *Arch. Microscop. Anat.* 9, 413 (1873), pp. 413.

[2] J.W. Lichtmann, *Spektrum der Wissenschaft* 78, (1994).

[3] P. Kruit (Hrsg), N. F. Hulst, A. Lewis, *Ultramicroscopy* 71, Elsevier, Amsterdam, Lausanne, New York, Oxford, Shannon, Tokyo (1998).

[4] E. H. Synge, *Philosophical Magazine and Journal of Science* 6, (1928), pp. 356-362.

[5] D. W. Pohl, W. Denk, M. Lanz, *Appl. Phys. Lett* 44, (1984), pp. 651.

[6] G.A. Valaskovic, M. Holton, G.H. Morrison, *Appl. Optics* 34 (1995), pp. 1215-1228.

[7] A. Sayah, C. Philipona, P. Lambelet, M. Pfeffer, F. Marquis-Weible, *Ultramicroscopy* 71, (1998), pp. 59-63.

[8] M. Ohtsu, *J. of Lightwave Tech.* 13, (1995), pp. 1200.

[9] R. Uma Maheswari, S. Mononobe, M. Ohtsu , *J. of Lightwave Tech.* 13, (1995), pp. 2308.

[10] Th Lacoste, Th. Huser, R. Prioli, and H. Heinzelmann *Ultramicroscopy* 71, (1998), pp. 333-340

[11] J. A. Veerman, A. M. Otter, L. Kuipers, N. F. Hulst, *Appl. Phys. Lett.* 72, (1998), pp. 3115.

[12] S. Pilevar, K. Edinger, W. Atia, I. Smolyaninov, C. Davis, *Appl. Phys. Lett.* 72, (1998), pp. 3133.

[13] E. Meyer and H. Heinzelmann, in *Scanning Tunneling Microscopy II*, 2nd Edn, ed. by R.Wiesendanger and H.-J. Güntherodt, Chapt. 4, pp. 101-103. Springer, Hamburg (1995).

2 Scanning Force Microscopy

2.1 Introduction

The scanning tunneling microscope (STM) and the scanning force microscope (SFM) are the two most widespread members of the SPM family. The first SFM also called atomic force microscope (AFM) was built in 1986 in California [1], four years after the development of the STM [2]. It consisted of a combination between a profiler and an STM. In contrast to the STM the AFM also allows the characterization of non-conducting surfaces. Topography images of surfaces with a resolution down to the atomic scale are now routinely achieved with commercial instruments.

The force sensor consists of a thin soft cantilever beam with a tip at its extremity. Very weak forces such as those acting between single atoms are measured by monitoring the deflection of this beam. Nowadays these probes are produced using silicon bulk micromachining. This fabrication technology has made it possible to build high quality probes with reproducible properties. Micromachining also enables deflection sensors or actuators to be integrated on the cantilever beam. Furthermore using microfabrication, probes with several cantilevers in parallel can be fabricated resulting in an increased imaging speed if operated simultaneously.

As this thesis deals with the fabrication of simultaneous AFM and SNOM probes, the working principle of AFM will be briefly explained along with different cantilever beam deflection measurement methods.

2.2 Functioning of an AFM

An AFM image is obtained by detecting weak forces acting between a tip and a sample. This is done using a force sensor (the AFM probe) consisting of a soft cantilever beam with a sharp tip at its extremity. When the tip is brought close to the sample surface, forces acting between the tip apex and the sample cause a bending of the cantilever. This cantilever deflection is detected and the signal is sent to a controller. The controller then generates a feedback signal for the scanner, the aim being to keep the deflection of the cantilever constant by moving the sample in the z direction. During scanning in x and y direction the amplitude of the feedback signal relative to its position on the sample is recorded in a computer (Figure 2.1). If contact forces are measured, this results in a high-resolution image of the topography of the sample.

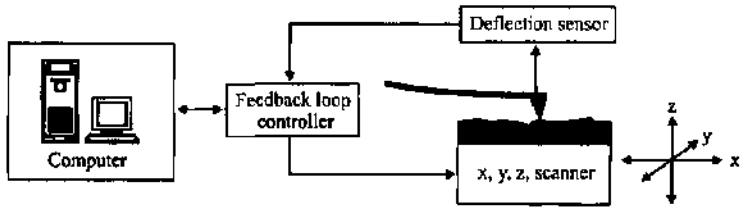

Figure 2.1: Schematic view of an AFM. The force is measured with a flexible cantilever beam. The cantilever deflection is detected and the force between the tip and the sample is kept constant during scanning by means of a feedback loop.

The forces acting between the tip apex and the sample are of different nature depending on the separation distance (Figure 2.2). When the tip is in contact with the sample surface, repulsive ionic forces are measured. If the distance is increased to a few nanometers longer-range attractive

forces such as van der Waals, capillary and electrostatic forces deflect the cantilever.

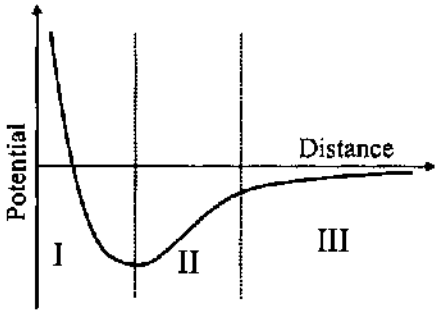

Figure 2.2: Qualitative representation of the potential encountered by a tip versus distance to the sample surface. In contact or very close to the surface, in regime I, repulsive forces are measured. In domain II and III longer range attractive forces are dominant.

The AFM can be operated in different distance regimes, such as contact mode and non-contact mode. Furthermore imaging can be done in quasi-static mode, or in dynamic mode depending on whether the cantilever is vibrated during scanning or not. Details about these techniques can be found elsewhere [3].

2.3 The AFM probe

For high resolution imaging the AFM probe must fulfill different conditions:

- The integrated tip must be very sharp. This is necessary for a good lateral resolution.
- The spring constant of the cantilever has to be small enough to detect weak forces.

- The resonance frequency of the cantilever must be high to allow fast scanning speeds. A high resonance frequency also makes the probe less sensitive to parasitic vibrations.

The seemingly contradictory conditions of high resonance frequency and low spring constant can be reunited by reducing the mass of the cantilever probe. This implies building probes that are small in size. Microfabrication has proved to be the best manufacturing method for probes with these properties [4, 5]. Most available commercial probes are fabricated using bulk silicon micromachining and molding techniques.

To increase the throughput several AFM probes can be operated simultaneously. This implies that each cantilever needs an individual actuation. Indeed as can be seen on Figure 2.3 the topography of the sample must be compensated for each cantilever separately. Also, when several cantilevers are operated in parallel, the deflection measurement method must be very compact. Integrating an actuator and a deflection sensor on each cantilever can solve this problem. A potential application for cantilever arrays is high-density data storage with increased throughput.

Figure 2.3: AFM imaging with several levers in parallel. Each cantilever must be actuated separately.

2.4 Deflection measurements

As previously mentioned the deflection of the cantilever must be measured very precisely. This can be done in different ways.

2.4.1 Laser beam deflection

The most commonly used method is the laser beam deflection method. Here a laser beam is focused on the backside of the cantilever and the reflection of this beam is directed to a segmented photodiode. When the cantilever is deflected the reflection of the beam changes its position on the photodiode [6]. This implies a change in the photo-current generated in each segment. This method is very simple, sensitive and easy to apply.

2.4.2 Interferometer

The cantilever deflection can also be measured by interferometry. This can be done, for example, by reflecting a laser beam from a closely placed optical fiber onto the backside of the cantilever [7, 8]. This measurement method is precise, however adjusting the fiber proves to be difficult.

2.4.3 STM tip

This method was chosen for the realization of the first AFM. A tunneling tip is mounted close to the backside of the cantilever and a voltage bias is applied [1]. High resolution is obtained by measuring the changes in tunneling current but as for the interferometer method, handling proved to be difficult. Furthermore, when performed in air, force measurements are not reliable.

2.4.4 Capacitance

A capacitance can be created by placing a rigid counter-electrode behind the cantilever. The cantilever deflection is then measured by the change in capacitance it induces. Because the capacitance can also be used for AC

and DC actuation, this detection method is suitable for the fabrication of cantilever arrays for parallel imaging [9, 10, 11]. Drawbacks of this method are a high sensitivity to noise and a small actuation amplitude.

2.4.5 Piezoresistive effect

The resistivity of silicon changes with applied stress. This effect can be used by placing a doped, U-shaped silicon resistor, on the cantilever base [12]. Such detection elements are very sensitive, easy to make, compact and have successfully been used for parallel imaging [13].

The gate of a CMOS transistor is also sensitive to stress and thus can be used as a deflection sensor. Details about this method can be found in [14].

2.4.6 Piezoelectric effect

A piezoelectric element integrated on the cantilever can be used for detection of the cantilever deflection as well as for actuation [15, 16, 17]. These probes are suitable for parallel imaging. However, their weakness lies in the quality of the piezoelectric material and the complicated fabrication process.

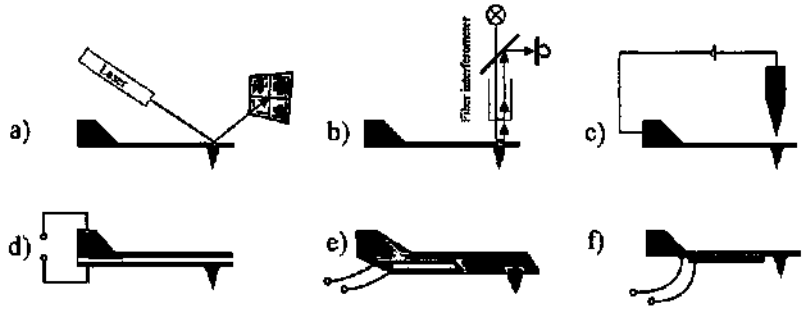

Figure 2.4: Different cantilever deflection measurement techniques. a) laser beam deflection, b) interferometry, c) tunneling tip, d) capacitance, e) piezoresistive, f) piezoelectric.

2.5 Conclusion

Scanning Force Microscopy is a well-established characterization method. Its flexibility and precision makes it a useful tool in many application fields.

The AFM probes are produced using silicon bulk micromachining technology. This same technology enables sensors and or actuators to be integrated on the cantilever. By doing this, measurements in vacuum or in a liquid environment are simplified. Also, the integration of actuators and deflection sensors makes it possible to increase the throughput by scanning with several cantilevers in parallel.

2.6 References

[1] G. Binnig and C.F. Quate and Ch. Gerber, *Physical Review Letters* 56, 9 (1986), pp. 930-933.

[2] G.Binnig and H.Rohrer, *Helvetica Physica Acta* 55, (1982), pp. 726.

[3] R. Wiesendanger, H. –J. Güntherodt, *Scanning tunneling microscopy II*, second edition, chapter 4, Springer-Verlag (1992).

[4] T. R. Albrecht, S. Akamine, T. E. Carver and C. F. Quate, *J. Vac. Sci. Technol.* A 8, 4 (1990), pp. 3386-3396.

[5] O. Wolter, Th. Bayer and J. Grescher, *J. Vac. Sci. Technol.* B 9, 2 (1991), pp. 1353-1357.

[6] G. Meyer and N. M. Amer, *Appl. Phys. Lett.* 53, (1998), pp. 2400-2402.

[7] D. Rugar, H. J. Mamin, R. Erlandsson, J. E. Stern and B. D. Terris, *Rev. Sci. Instrum.* 59, 11 (1988), pp. 2337-2340.

[8] C. Schönenberger and S. F. Alvaro, *Rev. Sci. Instrum.* 60, 10 (1989), pp. 3131-3134.

[9] T. Göddenhenrich, H. Lemke, U. Hartmann and C. Heiden, *J. Vac. Sci. Technol.* A. 8, 1 (1990), pp. 383-387.

[10] G. Neubauer, S. R. Cohen, G. M. McClelland, D. Horne and C. M. Mate, *Rev. Sci Instrum.* 61, 9 (1990), pp. 2296-2308.

[11] N. Blanc, J. Brugger, N. F. de Rooij and U. Dürig, *J. Vac. Sci. Technol.* B 14, 2 (1996), pp. 901-905.

[12] M. Tortonese, R. C. Barrett and C. F. Quate, *Appl. Phys. Lett.* 62, 8 (1993), pp. 834-836.

[13] S. C. Minne, S. R. Manalis, and C. F. Quate, *Appl. Phys. Lett.* 67, 26 (1995), pp. 3918-3920.

[14] T. Akiyama, A. Tonin, H. –R. Hidber, J. Brugger, P. Vettiger, U. Staufer, N. F. de Rooij, *Sensors and Actuators* A 64, (1998), pp. 1-6.

[15] K. Tanaka, *Jpn. J. Appl. Phys.* 32, (1993), pp. 2036-2038.

[16] T. Itoh, C. Lee and T. Suga, *Appl. Phys. Lett.* 69, 14 (1996), pp. 2036-2038.

[17] P.-F. Indermühle, G. Schürmann, G.-A. Racine, N.F. de Rooij. *Journal of Micromechanics and Microengineering* 7, (1997), pp. 218-220.

3 Principles of SNOM microscopy

3.1 Iotroduction

The resolution of standard optical microscopy is limited by diffraction to about half the wavelength of the light. This resolution can be drastically improved by reducing the size of the detector, and by decreasing the distance between the sample the detector, i.e. moving the detector into the near-field. Decreasing the distance between the sample and the detector allows one to collect evanescent (non-propagating) high order components of the optical field. Ideally both size of the detector and distance between the sample and detector should be much smaller than the wavelength of the observed light. This basic principle was proposed in 1928 already by Synge [1] followed in 1955 by O'Keefe [2]. But at that time technology was not sufficiently advanced to overcome the fabrication difficulties of such a microscope.

In this chapter, the working principle of SNOM and its different modes of operation will be explained. A good review concerning these subjects can be found in [3].

3.2 Near-field imaging

In a conventional optical microscope the image is formed by a succession of lenses which build an enlarged image from propagating light waves coming from the sample. Because of the wave nature of light and the finite size of the lenses, the resolution of such a system is always limited by diffraction. Abbe's [4] equation gives the minimum distance between two objects which can still be resolved:

$$\Delta X = \frac{0.61\,\lambda}{n \cdot \sin\theta} = \frac{0.61\,\lambda}{NA}$$

Equation 3.1: Abbe's equation showing the resolution that can be obtained with an optical system. λ is the wavelength of the light. NA is the numerical aperture of the lens system. NA is a function of the refractive index, n, and the maximum angle, θ, at which light can still enter the lens system.

A good standard optical microscope typically has a numerical aperture of NA = 0.9 in air (n =1). This leads to a maximum resolution of about 400nm for visible light.

In 1928 H. Synge proposed the following concept to get past the diffraction barrier. The idea is to illuminate the sample through a very small hole in an opaque screen and observe the transmitted light. The screen has to be brought into the near-field of the surface (at a distance much smaller than the wavelength of the light). The aperture is then scanned over the whole surface and the image is reconstructed during this probing.

The distance between the screen and the sample has to be much smaller than the wavelength of the light and kept as constant as possible during scanning. The resolution is, then, essentially determined by the diameter of the aperture. The whole imaging scheme can also be inverted and the sample illuminated globally from the backside. The aperture, then, acts as a small window through which the sample is observed.

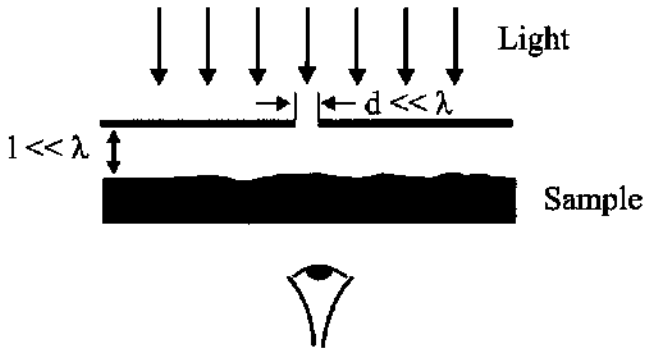

Figure 3.1: Basic principle of near-field microscopy as proposed by Synge. The sample is illuminated through a small aperture in an opaque screen, which is held very close to the sample surface. The transmitted light is observed from the backside.

During scanning, the aperture must stay within close and constant distance to the sample surface. This is difficult to do using a flat screen with an aperture, especially if the surface of the sample is not perfectly flat. Placing the aperture at the end a sharp tip ensures access to the sample and facilitates tbe distance control. As the intensity of the light transmitted through the aperture is very small, a powerful light source must be used in order to have enough signal. A laser light source is an obvious choice.

3.3 Modes of operation of a scanning near-field probe

3.3.1 Illumination mode

In this mode of operation, the aperture is used as a localized light source, which illuminates the sample. The light that reaches the detector contains the optical information of only a very small part of the sample surface. The tip is scanned over the sample and the image is reconstructed point by point. In this configuration the light source is in the near-field and the sample must be transparent. Illumination is the most commonly used imaging mode.

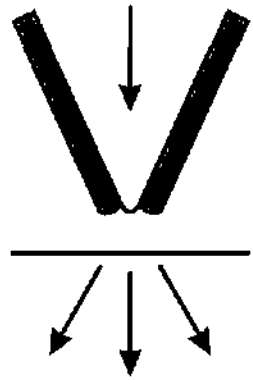

Figure 3.2: Operation in illumination mode. The aperture is used as a point source to illuminate the sample. Light transmitted through the sample is detected in the far-field.

3.3.2 Collection mode

This is the opposite configuration from the illumination mode. Here the aperture is used as a point-detector. The sample is illuminated in transmission from the backside, and only light that penetrates the tip through the aperture will be detected. In this imaging mode, the light is detected in the near-field. Only transparent or light emitting objects can be studied. This imaging mode is less suited for fluorescence imaging than the illumination mode. This is due to the fact that the sample is illuminated globally, which causes bleaching of the fluorescent dyes on a large surface.

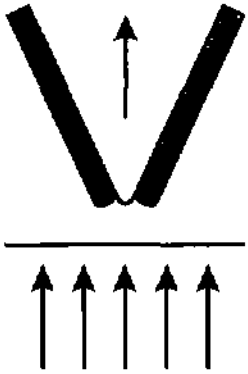

Figure 3.3: Collection mode. The sample is illuminated in transmission and light passing through the aperture is detected.

3.3.3 Reflection mode

This is the only SNOM mode, which can be used for the imaging of non-transparent samples. When the sample is illuminated through the probe the reflected light is either detected through the aperture (in the near-field) or by a detector placed sideways (in the far-field). However illumination can also take place from the side, the light being detected through the aperture. General problems are low signal intensity compared to the previously described methods because of weak collection efficiency. Also, when the probe is used for illumination and collection, the signal mixes with the illumination light reflected in the tapered region of the probe, making detection more difficult.

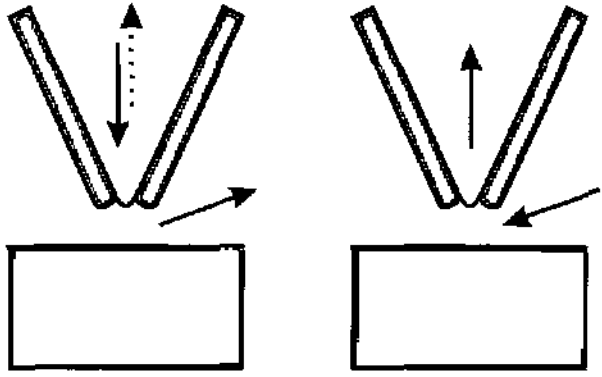

Figure 3.4: SNOM in reflection mode. When the sample is illuminated through the aperture, the reflected light is collected through the tip or by a lateral detector. It is also possible to illuminate the surface from the side and collect reflected light through the aperture.

3.3.4 Photon Scanning Tunneling Microscopy, PSTM.

An evanescent field is created on the sample surface by a total internal reflection. A dielectric tip scanned over the sample surface frustrates the total internal reflection and propagating waves are generated inside the tip. As the evanescent field decays very rapidly with distance imaging can also be done with a pointed probe having no aperture.

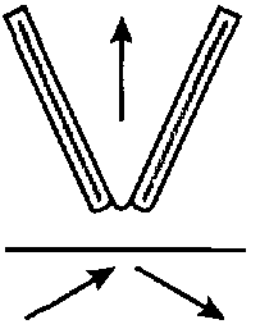

Figure 3.5: Photon Scanning Tunneling Microscope (PSTM). An evanescent field is created by total internal reflection, on the sample surface. The field is then probed by a dielectric tip with or without coating.

3.4 Conclusion

To be implemented, SNOM needs apertures to be fabricated in an opaque metal screen. Their size has to be in the nanometer range for visible light. For practical reasons, the apertures should be situated at the apex of a sharp dielectric tip. The fabrication of such a SNOM tip is a technological challenge, which has not yet fully been met. Main problems are reproducibility of aperture quality (size and shape).

3.5 References

[1] E. H. Synge, *Philosophical Magazine and Journal of Science* 6, (1928), pp. 356-362.

[2] J. A. O'Keefe, *Journal of the Optical Society of America* 46, 5 (1956), pp. 359.

[3] H. Heinzelmann, D. W. Pohl, *Appl. Phys.* A 59, (1994), pp. 89-101.

[4] E. Abbe, *Arch. Microscop. Anat.* 9, (1873), pp. 413.

4 Some optical characteristics of aperture probes

4.1 Introduction

An aperture probe is usually constituted by a tapered, metal covered, waveguide or a hollow metal tip. It is characterized by different parameters such as the aperture size and shape, which largely determines the resolution of the SNOM microscope, and optical transmission, which limits the maximum light intensity that can be emitted by the probe.

4.2 Optical transmission

When the probe is used as a localized light source, the transmission is the ratio between the optical power transmitted through the aperture and the total input power. In some particular applications such as nearfield optical data storage and high-resolution spectroscopy, high light intensities are an important issue.

The transmission through an ideal sub-wavelength aperture is proportional to the sixth power of its diameter [3]. However, the transmission not only depends on the aperture size but also on the geometrical shape of the probe tip and the material it is made of.

A SNOM tip is a tapered, metal covered waveguide. As light propagates towards the aperture a large part of the intensity is lost by backward reflections on the inclined side-walls of the probe. Furthermore, at some point, the width of the tapered waveguide reaches a critical diameter, called cut-off diameter, from where light propagation is strongly impeded

[1]. Light reaching this region of the probe will suffer vast losses. The metal constituting the coating of a real probe is not perfect. Thus, a part of the incident energy is dissipated and leads to local heating of the probe apex. For this reason, high light intensities cannot simply be achieved by increasing the input power. Indeed if a too high input power is used, melting of the metal layer, and destruction of the aperture can occur [2].

For a perfect waveguide with a perfect metal coating ($\varepsilon_{metall} = \infty$) the critical diameter d_c is expressed by [3]:

$$d_c = \frac{\lambda}{2n} = \frac{1}{2}\lambda_m$$

Equation 4.1: Critical diameter of a perfect waveguide. λ is the wavelength of light in vacuum and n, the refractive index of the dielectric material. λ_m corresponds to the material dependant wavelength.

This equation shows that the critical diameter is equal to half the material dependant wavelength of the light. This makes sense since the electric field at the interface to the perfect metal cladding must be equal to zero.

To increase the transmission of an aperture probe the high losses occurring in the region between the critical diameter and the aperture must be minimized. This can be done by fabricating SNOM probes with high refractive index materials and by increasing the taper angle of the probes. By using high refractive index materials like, for example, diamond and silicon nitride, the critical diameter is reduced and, thus, moves closer to the probe apex and aperture.

The other way of reducing the distance between the cut-off diameter and the aperture is to modify the taper angle of the aperture probe:

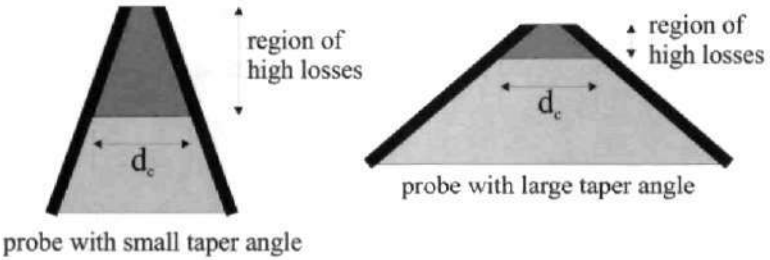

Figure 4.1: Comparison between two probe tips with same dielectric material but different taper angle. The probe with large taper angle has a higher transmission because the cut-off diameter is closer to the aperture.

In brief, the transmission of an aperture probe tip can be improved by using a material with high refractive index and by increasing the tip taper angle.

4.3 Effective aperture size

The aperture is the most important element of the SNOM probe. The size of the aperture has to be small for high-resolution imaging and its shape has to be well known to guarantee a well-defined optical interaction with the sample.

The choice of the metal used to fabricate the aperture is also important. The metal should have a high reflectivity in order to minimize the dissipation of energy and thus the heating of the probe apex (see paragraph 4.2). Directly linked to the reflectivity of a metal is its skin depth. The skin depth is the distance at which an electromagnetic wave can penetrate the metal until its intensity has diminished to a value of $1/e^2$

corresponding to 13 % of the original intensity [4]. This finite penetration depth determines an effective aperture size. A well-suited and thus widely used metal is aluminum. Aluminum has a short skin depth of 12.7 nm at $\lambda = 500$ nm. Thus the effective diameter of a 50 nm aperture structured into an aluminum layer is about 76 nm. This skin depth also limits the smallest possible effective aperture size to about 30 nm.

The thickness of the aluminum coating on the side-walls of the tapered probe is also important. It must be thick enough to ensure that the light transmitted through the metal cladding does not significantly contribute to the optical signal. In this work, the aluminum layers used for the coating of aperture probes have a nominal minimum thickness of 50 nm. An aluminum coating 50 nm in thickness attenuates the intensity of a light wave to about 4×10^{-4} of its original intensity.

4.4 References

[1] L. Novotny, C. Hafner, *Physical review* E 50, 5 (1994), pp. 4094-4106.

[2] D. I. Kavaldjief, R. Toledo-crow, M. Vaez-Irvani, *Appl. Phys. Lett.* 67, (1995), pp. 2771.

[3] J. D. Jackson, *Klassische Elektrodynamik*, 2 Auflage, Walter de Gruyter, Berlin, New York, Kapitel 8.3 (1982).

[4] M. V. Klein, T. E. Furtak, chapter 2 in *Optics*, second edition, John Wiley & sons, New York.

5 Conventional SNOM probes

5.1 Introduction

Most SNOM microscopes use specially processed optical fibers as near-field probes. The end of these fibers is shaped into a tip and an aperture is then patterned over it. These fibers can be used either as a localized light source or as a small collector. Distance regulation between the tip and the sample is achieved by the so-called shear force mode. In this mode the end of the fiber is oscillated laterally near its resonance frequency. When the tip comes close to the surface, forces acting between the tip and the sample damp the oscillation. The change in oscillation amplitude or frequency is monitored and used as a feedback signal to control the distance.

In this chapter fabrication methods for fiber-based SNOM probes will be presented along with the advantages and major flaws of this type of probes.

5.2 Shaping a fiber into a tip

There are two principal methods used to shape fibers into tips; by heating and pulling and by chemical etching. Both methods are serial processes. That means that no large number of probes can be fabricated in parallel.

5.2.1 Heating and pulling

In the first method the fiber is put under a mechanical strain while it is locally heated by means of a gas flame or a CO_2 laser (Figure 5.1). During pulling the fiber gets thinner and thinner until it eventually breaks, leaving a flat end at the apex. Parameters like pulling strength, pulling speed and heating power must be controlled precisely to fabricate sharp tips [1].

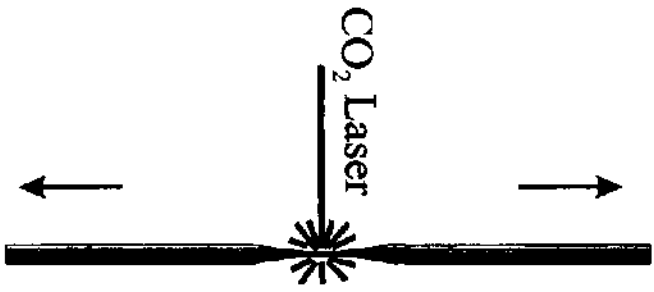

Figure 5.1: Fabrication of a tapered fiber. Simultaneous heating and pulling of the fiber forms the pointed ends.

Tips produced using this method are long and have a very small cone angle. Because of this, they are particularly fragile and their transmission is low, in the range of 10^{-5} to 10^{-6} [1]. However, the surface of these tips is very smooth which ensures a good quality of the metal layer that will be deposited for the aperture formation.

5.2.2 Chemical etching

The other method consists of chemically etching the fibers in an aqueous solution of Hydrofluoric acid (HF). The fiber is placed upside down in the etching solution, which is covered with a layer of immiscible solvent. The solvent protects the fiber after etching and prevents toxic and corrosive HF vapors from diffusing into the environment. The tip is formed at the interface between the acid and the solvent. Chemical etching allows the fabrication of tips with lager cone angles and thus several orders of magnitude higher transmission [2] than pulled fibers. Quite recently a technique was developed where the protective jacket of the fiber is left during etching [3]. This way the surface roughness usually encountered in chemical etching can be diminished (Figure 5.2).

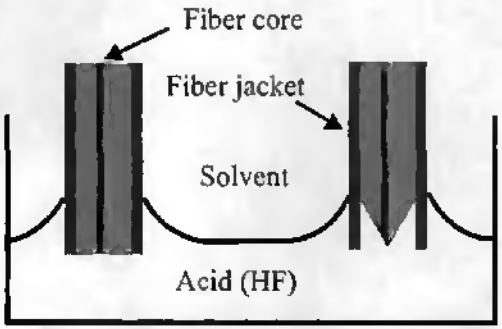

Figure 5.2: Chemical etching of optical fibers into tips. The fiber end is dipped into an etching solution without removing the protective jacket. Diffusion and capillary action lead to the formation of a tip.

5.3 Aperture formation

Once the end of the fiber is turned into a sharp tip, apertures are patterned into an opaque metal coating at the fiber-tip apex. The most common aperture fabrication methods giving good results are metal evaporation and Focused Ion beam (FIB) structuring. Because of its small skin depth (12.7 nm at λ = 500nm) aluminum is often chosen as coating material.

5.3.1 Metal evaporation

During metal evaporation the fibers are placed vertically in a holder and rotated as metal (usually aluminum) is evaporated at such an angle that the apex of the tip remains uncoated (Figure 5.3). Apertures fabricated by this method have an irregular shape because aluminum grains form at the rim of the aperture. During scanning the force interaction will most probably take place between one of these grains and the sample surface and so induce an offset between the topographical image and the optical image. Also the size of these apertures is not very reproducible.

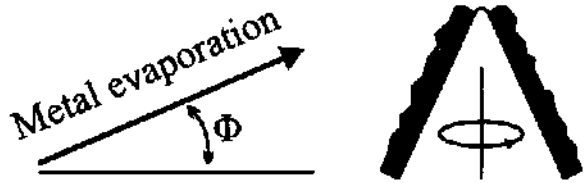

Figure 5.3: Metal is evaporated on a rotating fiber under an angle such that the tip apex is not covered.

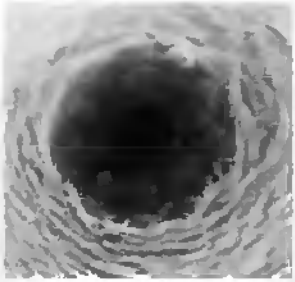

Figure 5.4: SEM image of an 100 nm in diameter aperture formed by metal evaporation. Note the presence aluminum clusters at the rim of the aperture. (courtesy Bert Hecht)

5.3.2 Focused Ion Beam (FIB)

A focused ion beam can be used as a tool to structure the apex of a fully metal covered tip. By aiming the beam laterally at the tip, its apex can be sliced away until the desired aperture size is achieved. A flat end then terminates the probe (Figure 5.5). Best results are achieved with this method. Another approach is to aim the beam vertically at the tip apex and drill a hole into the metal layer (Figure 5.1).

.

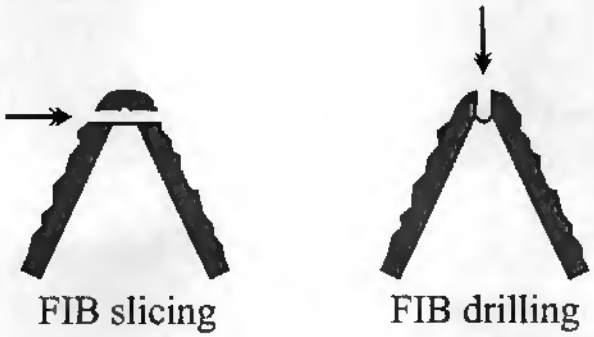

Figure 5.5: A Focused Ion Beam (FIB) can be used to slice away the top of a SNOM probe totally covered with metal, or to vertically drill a hole into the tip apex.

Apertures fabricated by Ion-beam milling have well defined geometrical properties. Their size and shape can be very well controlled but their fabrication is a very lengthy and costly process. Each tip must be processed individually in a series of cutting and observation cycles.

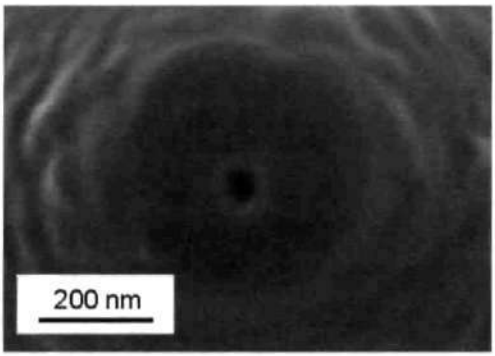

Figure 5.6: Top view of an aperture structured on a aluminum covered fiber using FIB slicing. (courtesy H. Heinzelmann)

5.4 Conclusion

One major drawback of these fiber–based probes is their fragility. Since the shear-fore distance control method implies that the fiber is placed vertically with respect to the sample surface it is very stiff and often breaks during scanning. By using special bent fiber probes the AFM distance control method can be applied [4,5,6]. However these probes are difficult to make and because of their stiffness they are inappropriate for some applications. A SNOM tip located at the end of a soft AFM-like cantilever could greatly improve this situation. Also the apertures fabricated by metal evaporation are not reproducible in size and shape. This is an important issue since the overall resolution of the SNOM microscope depends largely on these two parameters. Apertures fabricated

by Focused Ion Beam are nice but they are also very expensive and time consuming to produce because each tip must be processed individually.
All above presented fabrication methods are serial processes. This means no large amount of probes can be fabricated at the same time with reproducible properties. Microfabrication techniques have the potential to solve these problems. Also microfabrication technology could allow integrating the SNOM tip on AFM cantilevers and so improve the distance control and lifetime of a probe.

5.5 References

[1] G.A. Valaskovic, M. Holton, G.H. Morrison, *Appl. Optics* 34, (1995), pp. 1215-1228.

[2] A. Sayah, C. Philipona, P. Lambelet, M. Pfeffer, F. Marquis-Weible, *Ultramicroscopy* 71 (1998), pp. 59-63.

[3] P. Lambelet, A. Sayah, M. Pfeffer, C. Philipona, F. Marquis-Weible, *Applied Optics* 37, 31 (1998), pp. 7289-7292.

[4] S. Shalom, K. Lieberman, A. Lewis, S. R. Cohen, *Rev, Sci. Instrum.* 63, (1992), pp. 4061.

[5] H. Muramatsu, N. Chiba, K. Homma, K. Nakajima, T. Ataka, S. Ohta, A.Kusumi, M. Fujihira, *Appl. Phys. Lett.* 66, (1995), pp. 3245.

[6] C. E. Talley, G. A. Cooksey, R. C. Dunn, *Appl. Phys. Lett.* 69, (1996), pp. 3809.

6 Microfabrication of nanometer sized apertures

6.1 Introduction

The key component of every SPM probe is the SPM tip. General requirements for SPM tips are high aspect ratio, for good access to the sample and small radius of curvature at the tip apex, for high-resolution imaging [1]. An SNOM probe has one more demanding characteristic: its tip apex has to be fitted with a very small aperture structured into an opaque metal film. The size and shape of this aperture largely determine the resolution of the SNOM microscope. Making these apertures is one of the main difficulties encountered in the fabrication of a SNOM probe. This is also the case when microfabrication techniques are used. Most microfabrication techniques have been developed for flat surfaces and applying them to a structure as corrugated as a tip is not trivial. However, microfabricated probes have the potential to solve some of the problems of classical fiber-based SNOM probes, like reproducibility and quality and throughput.

In this chapter, the basic microfabrication techniques needed for probe fabrication will be presented along with different possible microfabrication approaches which allow to mass-produce SNOM apertures in a reproducible way. Finally a process involving a tip effect for the fabrication of SNOM apertures will be presented along with typical results.

6.2 Microfabrication techniques

All micromachining techniques have evolved from the technology developed for the fabrication of electronic circuits on slabs of monocrystalline silicon.

6.2.1 Standard photolithography

Photolithography is the process by which a geometrical pattern is transferred from a mask into a layer of photosensitive polymer covering the substrate. The polymer also called photoresist or simply resist, is sensitive to UV light and can be either "positive" or "negative" depending on whether the exposed parts are removed during development or not. The resist structures are then transferred into the underlying layer by a selective etching process which only attacks the unmasked parts of the substrate.

Instead of using the photoresist as a mask for etching, one can also use it as a sacrificial layer onto which the material that is to be patterned is deposited. The resist is then removed in a solvent and only the material deposited between the photoresist structures remains on the substrate. Since care must be taken not to destroy the resist structures, this so-called "lift-off" process can only be used for the structuring of materials deposited at low temperatures such as metals for example.

Photolithography is the basic procedure in microfabrication and usually precedes every step involving a chemical or physical etching of the substrate.

When higher resolution is needed other lithography methods exist such as Electron Beam lithography (E-Beam), or X-ray lithography.

6.2.2 Silicon bulk micromachining

Techniques have been developed that allow three-dimensional structures to be "carved" out of the silicon substrate. Here, the two most common silicon bulk micromachining methods are presented.

6.2.2.1 Anisotropic etching of silicon

Certain chemical compounds attack given crystallographic silicon planes faster than others. Potassium Hydroxide, KOH, is one of those substances [2]. This kind of anisotropic wet etching is often used to make well-defined three-dimensional silicon structures. The relative etching rate between crystallographic planes depends on the concentration of KOH in the etching bath and its temperature. The etching solution used during this work was an 40% aqueous KOH solution heated at 60°C. The materials used for masking during KOH etching are mainly silicon oxide and silicon nitride, because these materials show a high etch selectivity against silicon.

Silicon can also be etched isotropically in a mixture of nitric acid and hydrofluoric acid for example.

6.2.2.2 Dry etching of silicon

The term "dry etching" includes all etching techniques performed in a non-liquid environment. A reactive gas mixture, a plasma or an ion beam can all be used for the etching of silicon. Here we will focus on plasma etching, which is done in a reactor where a plasma is sustained.

There exist three different kinds of plasma etching modes depending on whether the ions of the plasma have a mechanical and, or, a chemical reaction with the silicon substrate.

During plasma etching the ions react chemically with the substrate forming a volatile compound. During Reactive Ion Etching (RIE) the ions

are accelerated towards the substrate and there is a chemical as well as mechanical action. During Ion milling, the ions do not chemically react with the silicon and the etching is only due to the impact of the ions.

Metals, silicon oxides or photoresist can be used as masking materials. A high selectivity and verticality is achieved by tuning the etching parameters such as, electrode power, substrate temperature, chamber pressure and gas flow.

Recently optimized reactors and processes have been developed for the etching of deep silicon structures [3,4]. These processes are called Deep Reactive Ion Etching (DRIE). They allow the microfabrication of high aspect ratio three-dimensional devices in higher density.

6.2.3 Silicon oxides and nitrides

With silicon being more or less conductive, it is sometimes necessary to electrically insulate some parts of the wafer. In most cases, silicon oxides and nitrides are used for this purpose.

Silicon oxide can be grown thermally or deposited by Chemical Vapor Deposition (CVD). Thermal oxide is grown by exposing a silicon substrate to oxygen or water vapor in an oven heated to about 1000°C. To obtain CVD oxide certain gases such as silane and oxygen are made to react in a reactor where the substrate is placed. This kind of oxide has the advantage that it can be deposited on other substrates than silicon and that its composition can be modified by adding other gases to the reactor. However the insulating properties of CVD oxides such as breakdown voltage are not as good as those of thermally grown oxide. Silicon oxide is mostly etched using a buffered solution of hydrofluoric acid called BHF. The buffer, NH_4F, ensures that the bath stays at a neutral ph and also increases the etching selectivity versus photoresist.

Silicon nitride layers are grown by Chemical Vapor Deposition. Because they are only very slowly etched in BHF, dry etching is the preferred structuring method.

Both silicon oxides and silicon nitrides can also be grown by Plasma Enhanced Chemical Vapor Deposition (PECVD) which allows lower deposition temperatures. Because of that, PECVD oxide and nitride can be deposited on a large variety of substrates.

6.2.4 Metals

In the majority of applications, electrical connections are made using structured aluminum lines. Aluminum is used for different reasons. First of all it is a good electrical conductor, and its adhesion properties on silicon and silicon compounds are good. Secondly, compared to other metals like gold for example, aluminum does not much diffuse into silicon when heated. This is very important since this process can damage the properties of electrical circuits.

Metals are mostly deposited by evaporation and structured by wet chemical etching or lift-off.

6.3 Different ways of making apertures

6.3.1 Electron-beam lithography

Electron-beam (E-beam) lithography is a versatile tool, which has the necessary precision and could allow to precisely control the size, position and shape of an aperture. The problems with lithography arise from the fact that it must be performed on the apex of a sharp tip. In order to achieve good resolution (below 100nm) the resist must be applied in a very thin and conformal coating. Its thickness should be of about the same size as the aperture. Such coatings can be formed by electrodeposition, electropolymerisation, or by precisely tuning the thickness of a photoresist layer by spinning (Figure 6.1). Unfortunately the chemistry of electropolymerisation and electrodeposition is quite complicated and it is very difficult to develop such a coating process for an E-beam resist. Adjusting the thickness of a photoresist layer by spinning, so that it barely covers the tip apex (Figure 6.2) is not a very flexible process because it must be tuned to a precise tip height and geometry. Alignment of the aperture with respect to the tip apex, during E-beam exposure, is also a very important but difficult task.

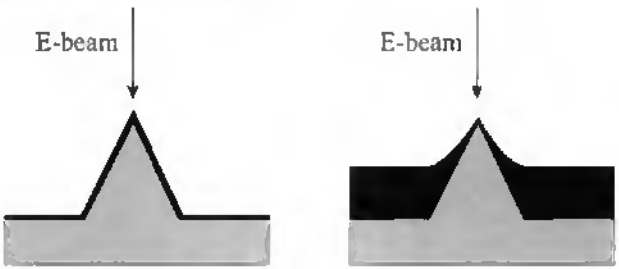

Figure 6.1: A thin conformal resist layer can be applied by electropolymerization (left figure), or resist can be spun on so it barely covers the tip apex.

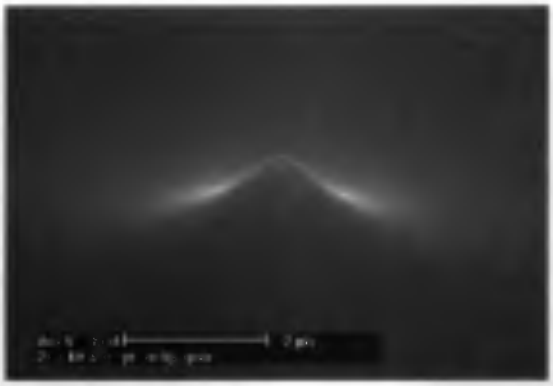

Figure 6.2: SEM picture of a silicon AFM tip covered with photoresist. The resist thickness has been adjusted so that it barely covers the tip apex. Such a layer would be suitable for E-beam exposure.

Advantages	+ Precise control of aperture shape and size
Disadvantages	- Resist coating difficult to apply
	- Spinning process dependant of tip height
	- Precise alignment of aperture necessary

Previous work in this field has been done by H. Zhou et. al. [5] who produced SNOM apertures on tips with a flat apex using electron-beam lithography and a special resist coating method.

6.3.2 "Thick" resist process

To avoid the burden of lithography, one can spin photoresist on the tips so that the apex protrudes, and use it as a mask to selectively etch an aperture into the metal film (Figure 6.3). However, again, the disadvantages are the dependency to tip height and tip geometry.

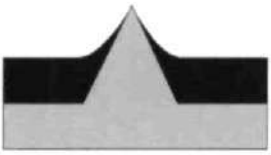

Figure 6.3: An optimized photoresist coating process leaves the tip apex uncovered, which can then be patterned.

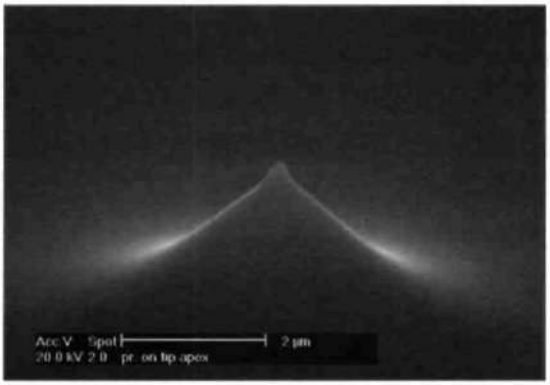

Figure 6.4: SEM micrograph of the situation described in Figure 6.3. The tip apex is protruding from the resist layer.

Advantages	+ No alignment necessary
Disadvantages	- Aperture shape depends on tip geometry
	- Spinning process dependant of tip height

6.3.3 Tip effects

Various tip effects like for example the enhanced electrical fields at tip apex due to the small radius of curvature can also be used as patterning methods.

Advantages: + No alignment necessary
+ Tip height independent
+ Very localized

Disadvantages - Aperture shape and size depends on tip geometry

6.4 Tip apex modifications using a tip effect

A tip effect during reactive ion etching (RIE) in a fluorine and chlorine ($C_2ClF_5 + SF_6$) containing plasma has been observed. This effect allows to selectively etch a silicon nitride layer only at the apex of a sharp tip. RIE is done in a reactor where a plasma is sustained between two electrodes by a radio frequency voltage. When the voltage is turned on, the different mobility of electrons and ions automatically induces a DC bias on the cathode, where the wafer is placed. The value of this DC bias is influenced by the gas flow, electrode power and chamber pressure. It can reach values of over 100V DC. The reactive gas ions present in the etching chamber are, hence, accelerated towards the surface and react with the substrate forming a volatile compound [6]. Due to the small radius of curvature, the electric field is higher on the tip apex than on the sidewalls. We believe that this field enhancement is responsible for the higher etching rate observed on the tip apex. Depending on the tip material, a layer CVD (chemical vapor deposition) nitride or PECVD (plasma enhanced chemical vapor deposition) nitride can be deposited on the tips. Then the coated tips are exposed to the plasma in the RIE reactor until the nitride is removed at the apex (Figure 6.5). This takes typically 1 minute etching time for 100 nm of nitride. If the etching is continued, the nitride will next be attacked also on the edges of the tip followed immediately by the side-walls (Figure 6.6). During the etching a DC bias voltage of 100V appears at the electrodes. Once patterned this structured nitride layer can be used as a mask for further processing steps.

Figure 6.5: Top view of a "knife edged" silicon KOH tip covered with silicon nitride. The nitride has been selectively removed on the ridge constituting the tip apex using a tip effect during RIE. The width of the ridge is estimated to about 70 nm.

Figure 6.6: Top view of a silicon tip covered with PECVD silicon nitride. The nitride on the edges and the side-walls of the tip has been damaged due to overetching.

6.5 SNOM apertures fabrication process

Using the previously described tip effect, an aperture fabrication process has been developed. The first step is the fabrication of a sharp tip, whereas the tip material can be silicon, silicon dioxide, silicon nitride, or even glass. Then a thin aluminum layer, about 50 nm in thickness is evaporated on the tip (Figure 6.7a). A 100nm thick layer of PECVD silicon nitride is deposited over the aluminum (Figure 6.7b). The silicon nitride layer is then patterned by means of the above explained tip effect in the RIE reactor (Figure 6.7c). In the last step, the silicon nitride is used as a mask to selectively wet-etch the protruding aluminum in a standard Al-etching solution, leaving a small aperture on the apex of the tip (Figure 6.7d). The shape of the aperture is determined by the tip geometry.

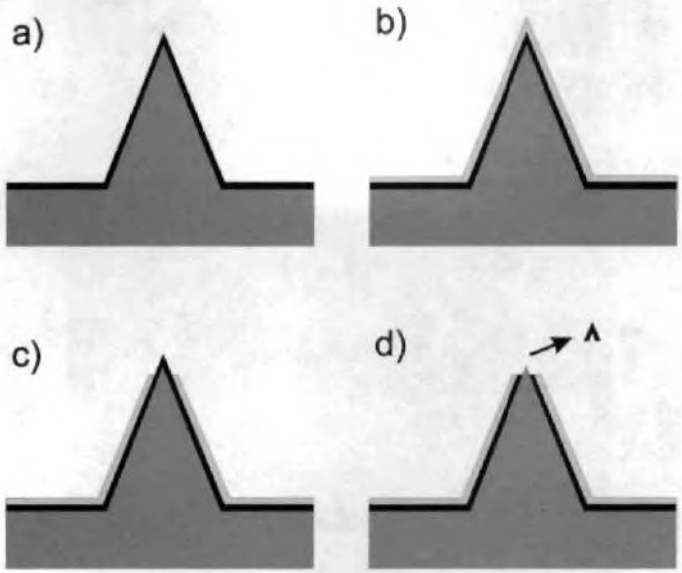

Figure 6.7: SNOM tips aperture fabrication process.

6.5.1 Results

The aperture fabrication process was first tested on 15 µm high silicon AFM tips. Figure 6.8 shows a side view such a silicon tip after the nitride has been selectively removed. This corresponds to step "c" in the previously described fabrication sequence.

Figure 6.8: SEM photograph of a tip after selective etching of the nitride. The tip apex is still covered with aluminum.

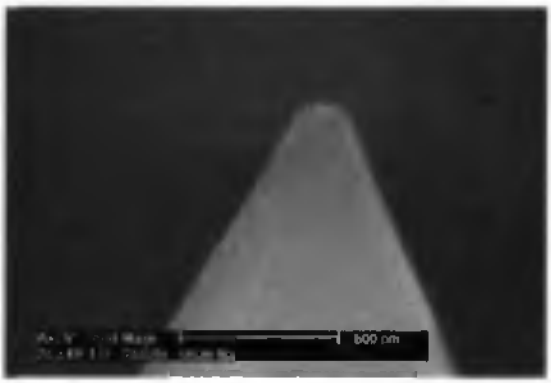

Figure 6.9: Same tip as in Figure 6.8 but after aluminum wet-etch. The arrow on the top image points at the Al-cusp, which is removed during the wet etching. The silicon nitride covering the rest of the tip acts a mask, protecting the underlying aluminum.

In Figure 6.9 the same tip can be seen after the aluminum etch (step "d" in fabrication process). This figure gives evidence that the little cusp in Figure 6.8 was actually formed by the underlying aluminum film, because it is removed by the Al-etchant, which does not attack the silicon nitride.

The following images show the flexibility of the aperture process regarding tip height and tip material. Using exactly the same fabrication parameters, apertures can be successfully made on 15 µm high silicon tips or 50 µm high quartz tips.

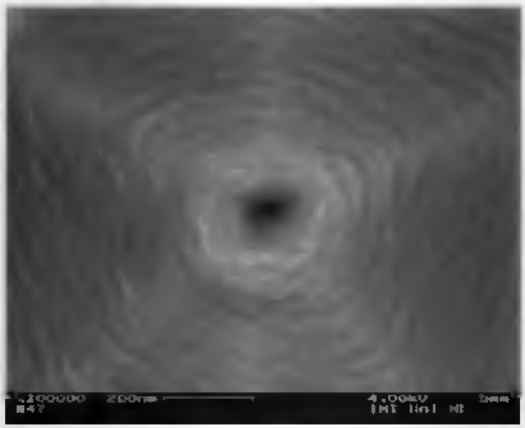

Figure 6.10: Top view of the aperture in an aluminum film covering a 15µm high silicon tip. To enhance contrast of the SEM image the silicon nitride has been completely removed from the tip. The aperture is estimated to be 50 nm in diameter.

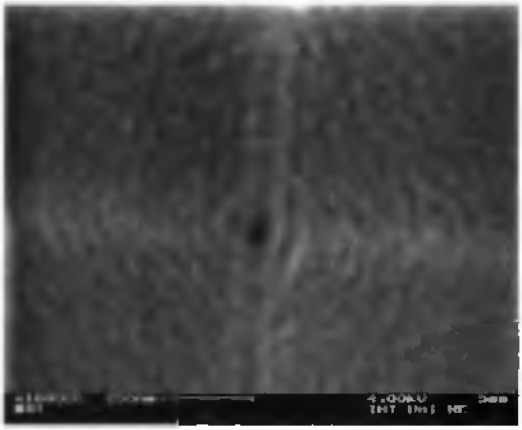

Figure 6.11: Top view of a 30 nm diameter aperture structured into an aluminum film on a 50μm high quartz (fused silica) tip. Silicon nitride has been completely removed from the tip.

This aperture fabrication method allows a full wafer of tips to be processed in parallel. The homogeneity of aperture size over a whole 4-inch wafer is good. The main problems encountered are homogeneity of tip shape. Since the process uses a tip effect, the shape of the very tip apex immediately determines the aperture shape. Because of that it is very important that the tips on which the apertures are to be patterned have a very well defined geometry at the apex.

6.6 Other SPM tips

By slightly adjusting the aperture fabrication process, different material contrasts can be produced at the apex of SPM tips. These modified SPM tips can find applications in various different fields.

6.6.1 Platinum nanoelectrode

Using the same process as for the SNOM apertures other SPM probes such as platinum nanoelectrodes can be fabricated. A silicon tip is first

coated with a 50 nm thick platinum layer. Then PECVD silicon nitride is deposited on top of the platinum and patterned according to the tip effect, resulting in a small protruding platinum apex (Figure 6.12). If the silicon nitride layer is thick enough, the protruding platinum apex is electrically isolated from the base. This small and well-defined electrode can be used e.g. for electrochemical measurements [7].

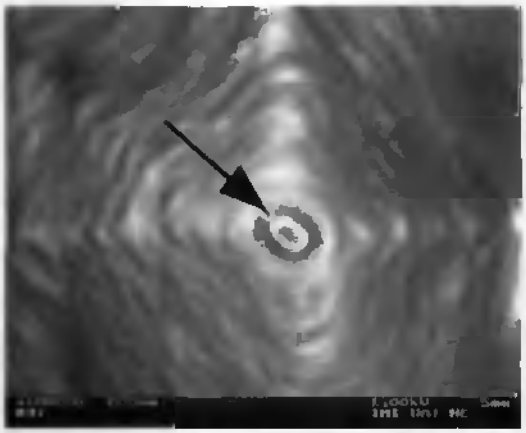

Figure 6.12: SEM micrograph of the apex of a platinum microelectrode. The arrow points at the protruding platinum apex which is about 100 nm long and 50 nm wide.

6.6.2 Nanocavities

Nanocavities can also be fabricated at the tip apex by adding an etching step to the aperture process. The patterned metal layer (Figure 6.7d) is simply used as a mask to etch the underlying silicon, by dry etching. Hollow metal tips with small apertures at the apex could be fabricated by simply removing the silicon totally.

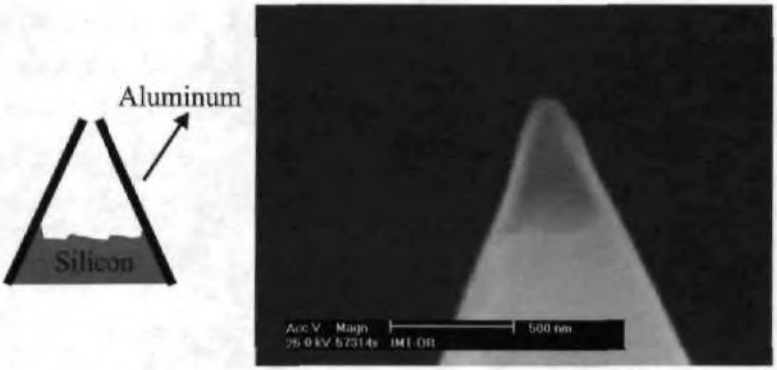

Figure 6.13: Side view of a nanocavity structured into a silicon tip.

6.7 Conclusion

The fabrication of nanometer-sized apertures at the apex of sharp tips can be done in different ways. However, the use of a structuring method based on a of tip effect seems to be the most promising.

The presented micromachining procedure is based on a tip effect that allows the batch processing the apex of microfabricated SPM tips on the nanometer scale. It relies on a tip effect in an RIE plasma and is fully CMOS compatible. It is simple, because it contains no lithography or alignment step. Furthermore it is not sensible to the tip height or to its material. The fabrication process is flexible, and can be used to fabricate other SPM probes such as platinum nanoelectrodes.

6.8 References

[1] M. Stedman, *J. of Microscopy* 152, (1998), pp. 611.

[2] H. Seidel, L. Csepregi, A. Heuberger, H. Baumgärtel, *J. Electrochem. Soc.* 137, (1990), pp. 3612-3626.

[3] STS ICP reactor.

[4] Alcatel CIT reactor.

[5] H. Zhou, A. Midha, G. Mills, S. Thoms, S. K. Murad and J. M. R. Weaver, *J. Vac. Sci. Technol.* B 16, 1 (1998), pp. 54-58.

[6] Marc Madou, *Fundamentals of Microfabrication*, CRC Press, Boca Raton, New York, (1997).

[7] M.I. Montenegro, A.A. Queiros, J.D. Daschbach, *Microelectrodes: Theory and Applications*, Kluwer, Dordrecht, The Netherlands (1990).

7 Aperture characterization

7.I Introduction

In the previous chapter a SNOM aperture fabrication process has been presented. Using this process apertures have been structured into aluminum films covering two different kind of tips: silicon AFM tips and quartz (fused silica) tips. As the resolution of the SNOM microscope largely depends on the quality of these apertures, their characterization is very important.

The size and shape of the apertures can be determined by SEM observation. However this kind of characterization does not take the optical behavior into account. The emission of light from an aperture can, for example, be influenced by inhomogeneities in the thickness of the metal coating or by the presence or absence of metal grains at the perimeter of the aperture. It is equally important that the metal coating is pinhole-free, since pinholes can modify the resolution of the SNOM microscope and raise the background signal level.

A certain amount of information about the optical characteristics of an aperture can be obtained by observing, in the far field, the image of light transmitted through the aperture.

7.2 Characterization of apertures structured on silicon AFM tips

The silicon AFM tips were fabricated using anisotropic etching in KOH, based on a process developed by Wolter [1]. Eight crystalline planes define the tips that are formed by this technique. A perfect tip has the eight planes intersecting exactly at the tip apex. Unfortunately this is not always the case and a "knife-edge" then terminates the tip. A study has shown that about 50% of all tips fabricated by this method are "knife-edges", whereas the other half is perfectly sharp [2]. Because the aperture fabrication process is based on a tip effect, "knife-edges" lead to elongated apertures with erratic shape. These kinds of apertures are not desired, in particular because the direction and length of the slit cannot be controlled.

7.2.1 SEM observation

As silicon is opaque to visible light, only SEM observation has been performed. During this study the mean size of the apertures was found to be around 70 nm with the smallest being 50nm in diameter and the largest in the 100 nm range. As can be seen in Figure 7.1 the apertures structured on "knife-edged" tips do not have a well-defined shape and are therefore not suited for SNOM imaging. No significant difference in aperture size was observed between the center and the edge of a processed 4-inch wafer.

The main problem encountered with aperture shape and size inhomogeneity is due to the inhomogeneity of the tips themselves. This could be improved by fabricating tips with a better defined tip apex [3].

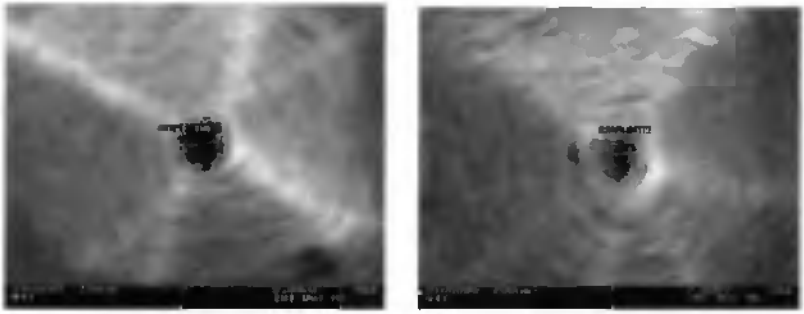

Figure 7.1: SEM images of typical apertures structured into a 50 nm thick aluminum layer covering silicon AFM tips. The left aperture is about 100 nm in diameter and the right one about 60 nm.

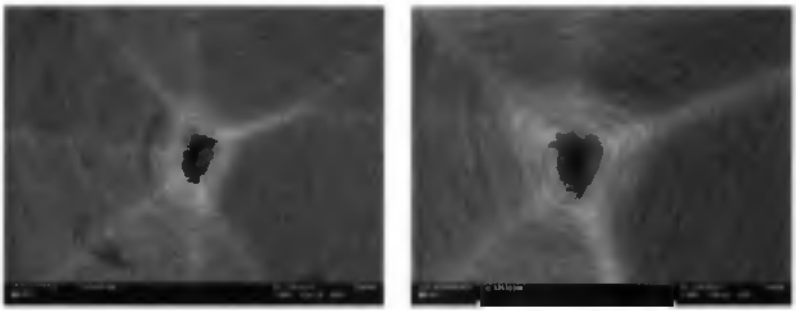

Figure 7.2: SEM images of apertures structured on "knife-edged" tips. The aluminum layer is 50 nm thick and the tips are 15 μm high.

7.3 Apertures on quartz tips

Quartz tips were fabricated on an amorphous fused silica wafer. They are isotropically etched in a concentrated hydrofluoric acid solution using polysilicon as mask material [4]. Tips fabricated by this method are extremely sharp and have a very low surface roughness (Ra of 5 Å to 10 Å), which is important for a high quality metal coating. They were produced using round, square and triangular mask shapes.

When square pads are used for tip fabrication, it often happens that the tip apex is shaped as a "knife-edge". This then results in apertures that are elongated in one direction. These "knife-edges" appear when the etching mask is not perfectly square, due to imperfections in the preceding lithography process. However, in contrast to the silicon KOH tips where the etching is sensitive to crystalline planes, it is possible to control the length and orientation of these "knife-edges" by creating very precise rectangular masks. Such elongated apertures could specifically be used for their polarization dependent transmission properties [5]. Tips shaped from round and triangular masks avoid this "knife-edge" problem.

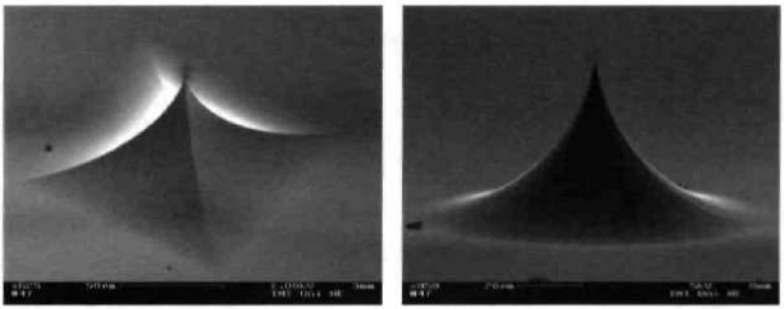

Figure 7.3: SEM pictures of quartz tips produced by under-etching of a square and a round mask.

7.3.1 SEM characterization

The size of the apertures structured on quartz tips was measured using SEM observation. From these observations one can say that their diameters vary between 30 nm and 100 nm. Whereas most apertures are in the 50 nm to 80 nm range. The aperture size and shape homogeneity is good, mainly because the tips themselves have a well-defined tip apex geometry. The opaque metal coating is constituted by a 5 nm thin adhesion promoting titanium layer and a 100 nm thick aluminum layer.

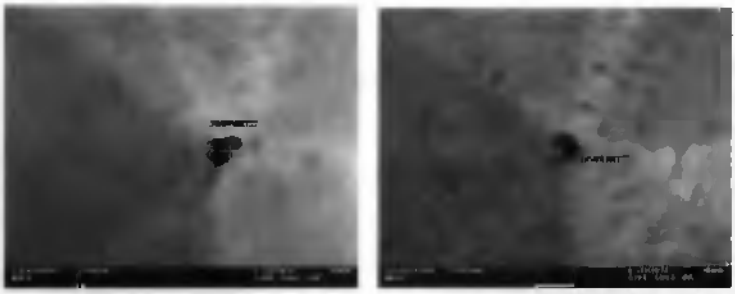

Figure 7.4: SEM pictures of apertures structured on quartz tips fabricated from circular masks. The apertures are estimated to be about 70 nm in diameter.

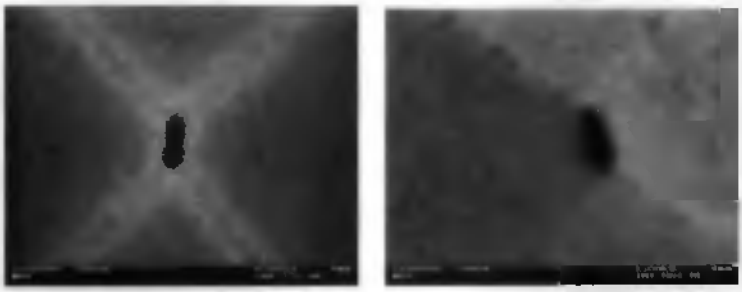

Figure 7.5: SEM micrograph of elongated apertures about 150nm long and 70 nm wide. In this case a square mask has been used for the tip fabrication.

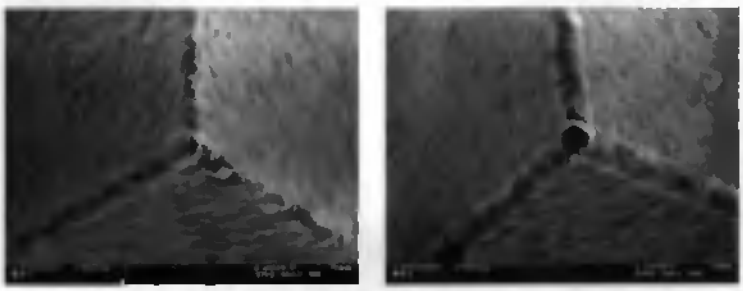

Figure 7.6: Pictures of the apex of triangular tips. The apertures are not clearly seen on these photographs however their presence is proved by optical characterization (see below).

7.3.2 Optical characterization

In order to characterize the apertures optically, the tips were used in transmission and the emission pattern was observed in the far field. To do so an optical setup was built which allows a laser beam to be focused into the tip from the backside by means of a microscope objective (20x, Na 0.35). The light transmitted through the aperture is collected with another microscope objective (100x, Na 0.9) and projected on a CCD camera. Polarizing filters are placed between the laser source and the first microscope objective as well as between the second microscope objective and the camera. The first filter allows the intensity of the incident laser beam to be regulated. By varying the direction of the second filter it is possible to look at how the polarization of the light is affected by the aperture. As the apertures are much smaller than the wavelength of the light source (He-Ne laser at 633 nm), they are expected to behave like point light sources.

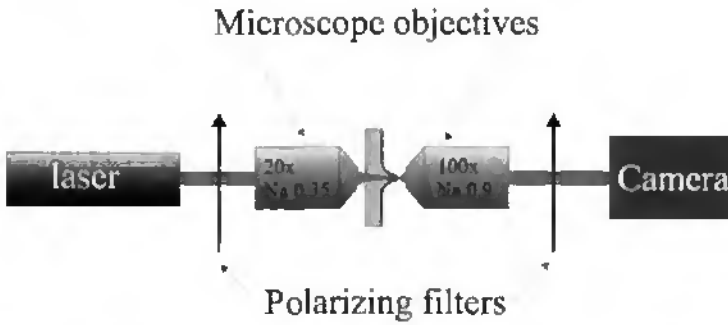

Figure 7.7: Schematic view of the optical aperture characterization setup. A laser beam is focused into the back of the tip with a microscope objective. The transmitted light is imaged using a high numerical aperture microscope objective and projected on a CCD camera.

7.3.2.1 Numerical calculations of the emission pattern

For comparison with experimental results, the emission pattern of a perfect aperture, as seen with the above presented characterization setup, was calculated numerically. These calculations were done by W. Noell and performed in three steps. First the electric field inside the aperture is calculated. Then the value of the field once it has propagated to the microscope objective is calculated. And finally the diffraction induced by the microscope objective is taken into account. In the following calculations the light waves propagate along the optical axis, in the z direction, and are polarized perpendicular to the optical axis, in x and y.

For simplifying the calculations the emission from the tip is assumed to satisfy the equations derived by Bethe [6] and Bouwkamp [7]. The Bethe-Bouwkamp approximation [8] is valid for a circular aperture surrounded by a thin perfectly conducting metal and illuminated from the back by a plane wave polarized in the x-direction. Figure 7.8 shows the calculated intensity of the field at the aperture for both polarizations, parallel (x-polarization) and perpendicular (y-polarization) to the incident plane wave polarization.

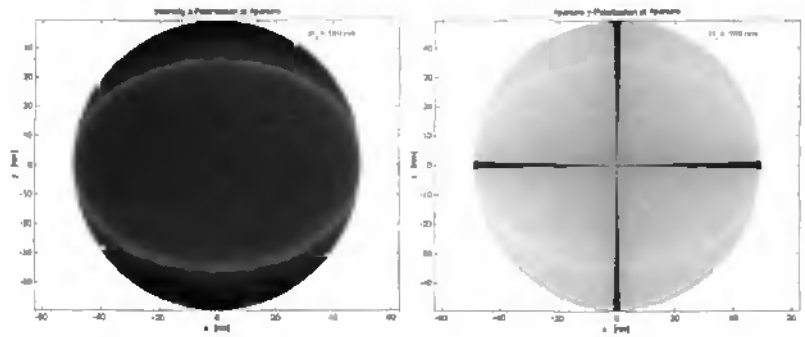

Figure 7.8: Calculated intensity of the electric field in logarithmic scale for x-polarization and y-polarization inside a circular aperture 100nm in diameter using the Bethe-Bouwkamp approximation.

From the aperture the field freely propagates to the microscope objective. The propagation was calculated following the Huygens principle. This principle states that each point on a wavefront generates a spherical wave. The superposition of these waves constitutes the wave at another point (see diffraction integral in chapter 6 of [9]). The following calculations present the field as it is at the microscope objective. These results are in good agreement with calculations performed elsewhere [10].

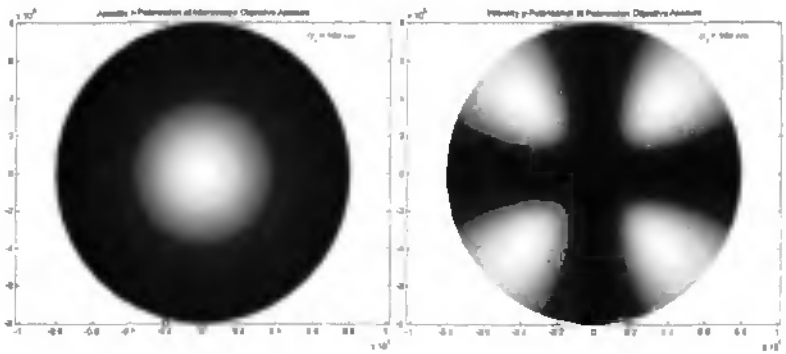

Figure 7.9: Intensity at the microscope objective for both polarizations. This field was calculated by propagating the previously calculated field from the aperture towards the microscope objective.

The microscope objective acts as an aperture, diffracting the field, which then propagates further to the CCD camera. Again Huygens's principle was used for this operation. In the following figures the calculated field at the CCD camera is compared with real images obtained from apertures structured on round quartz tips. These two patterns contain qualitative information about the optical shape of the aperture but not about it's size.

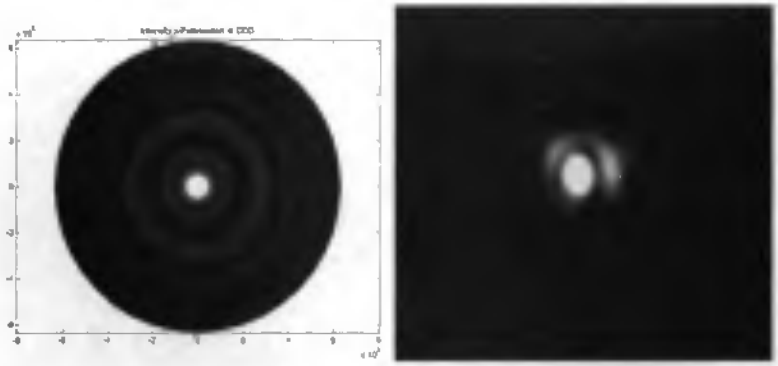

Figure 7.10: Comparison between calculated and measured x-polarization intensity at the CCD camera.

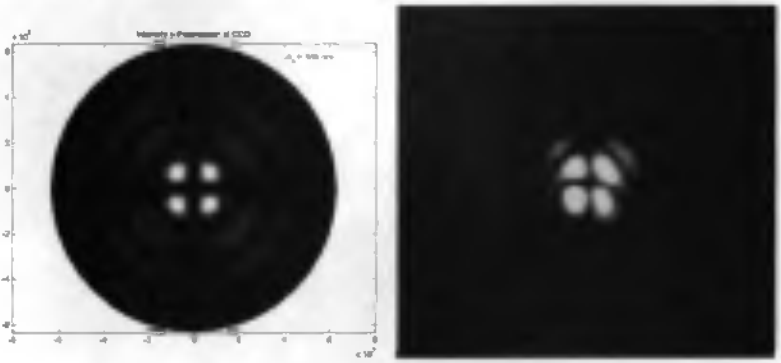

Figure 7.11: Comparison between calculated and measured y-polarization intensity at the CCD camera.

As can be seen in Figure 7.10 and Figure 7.11 there is a good agreement between calculated and experimental images. From this it can be concluded that the aperture that produced these images is almost round in shape and of good optical quality. The better the experimental image corresponds to the calculated pattern the closer the aperture approaches a perfectly round aperture.

Figure 7.12 shows the emission pattern obtained from an elongated aperture structured on a square quartz tip. A clear difference with the pattern obtained from a round aperture can be observed.

Figure 7.12: Emission pattern of an elongated aperture structured on a square quartz tip. The left image is the field component polarized parallel to the incident beam polarization (x-axis) and the right image is the component along the y-axis.

The emission patterns obtained from apertures structured on triangular tips are of very interesting shape. In particular the field intensity for the x-polarization shows multiple maximums. More extensive investigations need to be undertaken to prove their suitability for SNOM imaging.

Figure 7.13: Emission images of an aperture on a triangular tip for x-polarization (left image) and y-polarization.

7.3.3 Transmission

The transmission of the quartz tips was measured by replacing the camera of the optical characterization setup with a photodiode. Typical transmission values of apertures around 60 nm in diameter structured on round tips were found to be in the order of 10^{-5}.

7.4 Conclusion

Apertures have been fabricated on two different types of tips: silicon AFM tips and quartz tips. The aperture size uniformity is good and mainly depends on the tip apex geometry. Most fabricated apertures have diameters in the range of 50 nm to 80 nm. A problem for aperture fabrication on silicon AFM tips is the random appearance of "knife edges" during the tip fabrication. An improved tip fabrication process is necessary to obtain a better yield of usable apertures. Changing the mask shape, in order to obtain tips that are defined by three silicon crystalline planes could solve this problem. Other possibilities are the fabrication of tips by isotropic etching or the subsequent sharpening of the tips to remove the "knife-edges".

The microfabricated quartz aperture tips seem to be well suited for SNOM imaging and the emission patterns of round tips are in good agreement with numerical calculations. Thus, one can expect that these tips are polarization maintaining. The emission pattern gives qualitative information about the shape of the aperture. Triangular tips show a particular emission pattern and their suitability for SNOM imaging needs to be evaluated. Elongated apertures can be fabricated by etching tips with a rectangular mask. Such apertures could be used for studies with polarized light.

7.5 References

[1] O. Wolter, Th. Bayer, and J.Greschner, *J. Vac. Sci. Technol.* B 9, 2 (1991), pp. 1353-1357.

[2] C. Beuret, Ph. Niedermann, U. Staufer and N. F. de Rooij, *Microelectronic Engineering* 41/42, (1998), pp. 543-546.

[3] See for example, Diploma Work of G. Niederer, "Etching of trilateral silicon tips and realisation of a linear guide", University of Neuchâtel Switzerland, (1999).

[4] M.-A Grétillat, F. Paoletti, P. Thiébaud, S. Roth, M.Koudelka-Hep, N.F. de Rooij, *Sensors and Actuators* A60, (1997), pp. 219.

[5] E. Oesterschulze, O. Rudow, C. Mihalcea, W. Scholz, S. Werner, *Ultramicroscopy*, 71, (1998), pp. 85-92.

[6] H. A. Bethe, *Phys. Rev.* 66 (1944), pp. 163.

[7] C. J. Bouwkamp, *Rep. Phys.* 27 (1954), pp. 35.

[8] D. Van Labeke, F. Baida, D. Barchiesi, D. Courjon, *Optics Communications* 114, (1995), pp. 470-480.

[9] M. V. Klein, T. E. Furtak, *Optics*, second edition, John Wiley & sons, New York.

[10] P. K. Wei, R. Chang, J. H. Hsu, S. H. Lin, W. S. Fann, B. R. Hsieh, *Optics Letters* 21, 23 (1996), pp. 1876-1878.

8 Microfabricated SNOM probes

8.1 Introduction

Microfabrication techniques have promoted the breakthrough of AFM microscopy by providing high-quality probes with well-defined and reproducible properties. These probes are fabricated using silicon bulk micromachining. SNOM probes can be produced with the same technology. The most interesting aspect is that the SNOM tip can be integrated on an AFM cantilever. It is then possible to benefit from the precision, reliability and ease of use of the AFM distance control method. Furtbermore, microfabrication will allow adding deflection sensors and actuators to the cantilever, thus opening the possibility for parallel imaging.

Different possibilities exist for measuring the deflection of a cantilever (see chapter 2). The most widely used method in AFM microscopy is the beam deflection method. However, if used during simultaneous AFM and SNOM imaging, optical methods such as the beam deflection or the interferometer method may generate some unwanted background signals. By using other deflection measurement methods such as the piezoresistive or piezoelectric effect this problem can be solved.

Two basic approaches have been pursued for the fabrication of combined SFM and SNOM probes using silicon micromachining technology:

- One approach consists of detecting the light in the probe itself, by integrating a light sensor.
- The other approach is to integrate a transparent or hollow SNOM tip on a SFM cantilever.

8.2 The "active" probe

The optical signal can be directly detected inside the tip by an integrated light sensor, thus, no collecting optics are needed. An opaque metal film into which an aperture is structured at the apex spatially limits the interaction of the photons with the integrated sensor (Figure 8.1). The sensor signal is proportional to the intensity of the light penetrating the tip. Thus it is possible to make a high-resolution optical intensity image of the sample surface. One disadvantage of such a probe is that other optical information like polarization or wavelength can not directly be detected. Previous work in this field has been done by R. C. Davis et al. who integrated a Shottky diode into a silicon tip [1]. Instead of silicon other groups have used gallium arsenide as material for the tip into which the Shottky diode was integrated [2]. Another group has fabricated a cantilever with an integrated photodiode and added a plain micro-tip. Light scattered by the tip off the sample surface is detected by the photodiode [3].

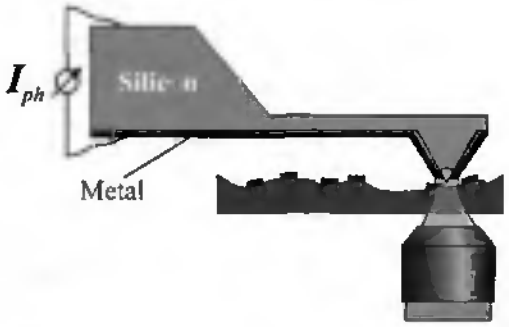

Figure 8.1: Schematic view of a microfabricated AFM cantilever with photosensitive Shottky tip. An aperture in an opaque metal coating covering the tip confines the light detected by the photosensitive element. The photocurrent I_{ph} as a function of the tip position on the sample gives the optical image. The sample is illuminated in transmission.

8.2.1 The "passive" probe

In another approach, a transparent or hollow tip is integrated on an AFM cantilever and used to illuminate the sample or collect light through the aperture at the apex. Figure 8.2 shows a schematic view of such a probe where the opaque cantilever has an opening located on the backside of the tip. When imaging in illumination mode, light is focused into the base of the tip and the sample is illuminated through the aperture. The scheme can be inverted for collection mode. With these probes it is possible to use all the different optical information, like polarization, phase contrast and wavelength. W. Noell et al [4] have fabricated a similar device. They have integrated a transparent silicon nitride tip on a cantilever. The light is brought to the tip and the aperture at the apex by a wave guiding structure added to the cantilever. Others have modified silicon nitride SFM cantilevers and added a metal coating with an aperture to the tip [5,6]. Hollow tips with an aperture at the apex have also been successfully used for SNOM imaging [7, 8, 9].

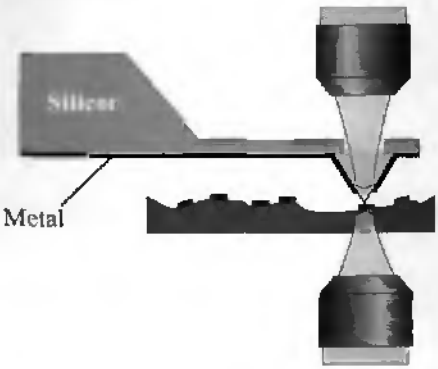

Figure 8.2: Schematic view of an AFM cantilever with integrated dielectric tip. A small aperture has been machined into a metal layer at the apex of the transparent tip. An opening in the cantilever, behind the tip, allows light to be detected or focused into the tip. Transmission and Illumination mode images can be made with such a type of device.

In the following chapters the fabrication process of two different probes will be presented. One probe consists of a silicon AFM cantilever-probe with integrated p-n junction. The other is a quartz tip added to a silicon AFM cantilever.

8.3 References

[1] R. C. Davis ,C. C. Williams and P.Neuzil, *Appl. Phys. Lett.* 66 , 2309 (1995).

[2] S. Heisig, H.-U. Danzebrink, A. Leyk, W. Mertin, S. Münster, E. Oesterschulze, *Ultramicroscopy* 71, 1-4, (1998), pp 99-105.

[3] Y. Tanaka, K. Fukuzawa and H. Kuwano, *J. of Appl. Phys.* 83, 7 (1998), pp. 3547-3551.

[4] W. Noell, M. Abraham, K. Mayr, A. Ruf, J. Barenz, O. Hollricher, O. Marti and P. Güthner, *Appl. Phys. Lett.* 70, (1997) pp. 1236.

[5] M. Radmacher, P. E. Hillner, P. K. Hansma, *Rev. Sci. Instrum.* 65, 8 (1994), pp. 2737-2738.

[6] A. G. T. Ruiter, M. H. P. Moers, and N. F. van Hulst, *J. Vac. Sci. Technol.* B 14, 2 (1996), pp. 597-601.

[7] H. Zhou, A. Midha, G. Mills, S. Thoms, S. K. Murad, J. M. R. Weaver, *J. Vac. Sci. Technol.* B 16, 1 (1998), pp. 54-58.

[8] Phan Ngoc Minh, Takahito Ono, Masayoshi Esashi, *IEEE*, (1999), pp. 360-365.

[9] E. Oesterschulze, O. Rudow, C. Mihalcea, W. Scholz, S. Werner, *Ultramicroscopy* 71, (1998), pp. 85-92.

9 Fabrication of an AFM cantilever probe with integrated p-n photodiode

In this chapter the fabrication of a combined SFM and SNOM probe will be presented. It consists of an AFM type micromachined silicon cantilever with an integrated silicon tip. A photodetector, more precisely a p-n junction, is built into the measuring tip as well as into a reference tip, which is located on the bulk of the chip. The measuring tip is covered with an opaque aluminum film into which an aperture is etched. The aperture is located on the apex of the silicon tip. It confines the light detected by the integrated photodiode to a small area. The reference tip is completely covered with a thick opaque metal layer. This reference tip will allow making differential measurements in order to compensate for aging and thermal drifts of the sensor signal.

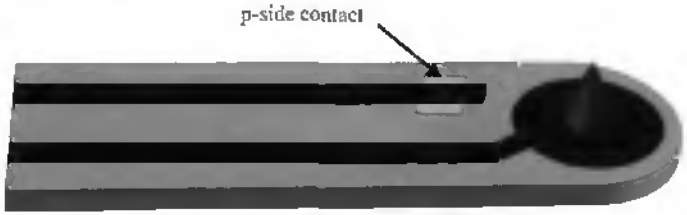

Figure 9.1: Schematic view of the cantilever extremity with the measuring tip. The two black aluminum lines contact both sides of the p-n junction. The tip is covered with a thin aluminum layer that serves as contact to the n-doped tip and as opaque metal layer into which the aperture is patterned.

In previous work, other groups have integrated Shottky diodes as light sensors [1, 2] into microfaricated tips. Shottky diodes have one advantage over p-n junctions: the light sensitive region is located at the interface between the metal and the semiconductor, thus, close to the semiconductor surface. However, a higher light sensitivity can be achieved with optimized p-n junctions. In future designs the p-n junction could be substituted for even more sensitive p-i-n or avalanche photodiodes.

9.1 Fabrication sequence

The wafers used for the fabrication of the probes are SOI (Silicon On Oxide) wafers with a 22 μm thick, p-doped, device layer. This device layer which has a resistivity of 0.03 /cm^2 is highly doped to ensure that ohmic contacts will immediately form between the aluminum electrodes and the silicon substrate and so, limit the number of processing steps.

9.1.1 Tip fabrication and back-side patterning (Figure 9.3, a)

After cleaning, a layer of thermal silicon dioxide is grown on the wafer, followed by the deposition of LPCVD (Low Pressure CVD) silicon nitride. Then by lithography the patterns for the tip etching are defined on the top surface. The dry etching of the silicon nitride and the removal of the underlying oxide by wet chemical etching in BHF follow this lithography step. Before the tips are formed, the nitride on the backside of the wafer is also structured by lithography and dry etching. These nitride patterns will be used as masks during the final step of the fabrication process. Tips are then etched in potassium hydroxide (KOH), based on a process developed by Wolter [3] (Figure 9.3, a). Square pads 60μm per

side are used as masks for the tip formation. The height of the tips varies between 13 and 15 µm.

9.1.2 Formatioo of the photodiode (Figure 9.3, b)

A layer of n-doped CVD (chemical vapor deposition) silicon oxide is deposited on the wafer surface. This layer is then structured so that an oxide pad is left on the tip. A special lithography process involving a 40 µm thick photoresist layer [4] is used for this purpose. Thick photoresist must be used because the tips have to be fully covered with resist during the wet etching of the oxide in BHF. The wafers are then heated in an oven at 1100 °C and the phosphor diffusing out of this doped silicon oxide layer into the p-type substrate forms the p-n junction (Figure 9.3, b). The superfluous oxide can then be completely removed by wet etching.

9.1.3 Cantilever formation (Figure 9.3, c)

Using a deep reactive ion etching the cantilevers are cut out (Figure 9.3, c). The buried oxide of the SOI wafer serves as an etch stop. By doing this the thickness of the cantilevers is well defined and uniform. Here again the lithography step preceding the dry etching is done using 40 µm thick photoresist. This is necessary since one wants to avoid blunting the tips during the etching [5].

9.1.4 Patterning of the electrodes (Figure 9.3, d)

A PECVD silicon nitride layer is deposited on the topside of the wafer. Using photolithography and BHF etching an access to the p-type substrate is made close to the tip. As normal resist (2.5 µm in thickness) is used, the tip is not totally covered and the nitride is also removed from the upper

half of the tip during the etching. This structured nitride layer serves to insulate the electrodes from the substrate and avoid short circuiting the photodiode. Here, PECVD silicon nitride is used instead of LPCVD nitride because it can be easily removed from the tip apex by wet etching without damaging it like with dry etching.

Aluminum is then evaporated on top of this nitride layer and the electrodes are patterned (Figure 9.3, d). Again, standard resist and wet chemical etching is used for this purpose. This thick aluminum layer now also covers the reference tip whereas the measuring tip is free.

9.1.5 Aperture formation (Figure 9.3, e, f)

A 50nm thick aluminum layer is evaporated over the tip, and structured using the thick photoresist process and wet etching. This aluminum layer, covering the tip, acts at the same time as a contact to the n-doped side of the junction, and as opaque layer into which the light confining aperture will be structured (Figure 9.3, e). The apertures are fabricated according to a previously described tip structuring process. In this batch fabrication method, a 100 nm thick silicon nitride layer is deposited on the metal covered tip and structured using a tip effect during RIE [6]. This silicon nitride layer is then used as a mask to etch the aperture into the metal film (Figure 9.3, f).

9.1.6 Releasing of the cantilevers (Figure 9.3, g, h)

In order to be able to access the metal electrodes, the nitride is removed from the contact pads by etching in BHF (Figure 9.3, g). Again, thick resist is used to protect the tip as BHF will also etch the silicon nitride and the thin metal layer into which the apertures are structured.

Finally the backside of the wafer is etched in KOH, and the cantilevers are released (Figure 9.3, h). The buried silicon oxide layer is used as an etch-stop and later removed in BHF, the front side being protected by photoresist. During etching the wafer is placed in a chuck which protects the topside. For this purpose, a special chuck was developed (Figure 9.2). It consists of a steel ring with a transparent plastic cover. A gap between the cover plate and the wafer has been added so that the tips can not be damaged by contact with the plastic cover. Also a slight overpressure of nitrogen can be applied to this volume. By doing so, KOH is prevented from leaking into the chuck through scratches or cracks in the nitride mask.

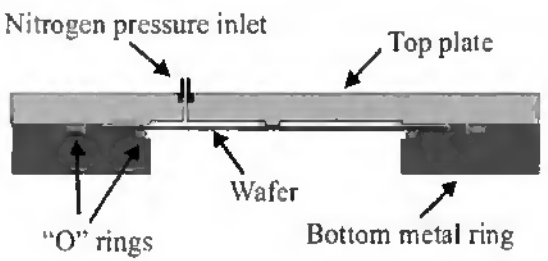

Figure 9.2: Schematic of the modified chuck for KOH etching. A gas inlet permits to apply a slight nitrogen pressure to the spacing between the wafer and the top plate. By this method small leaks can be avoided.

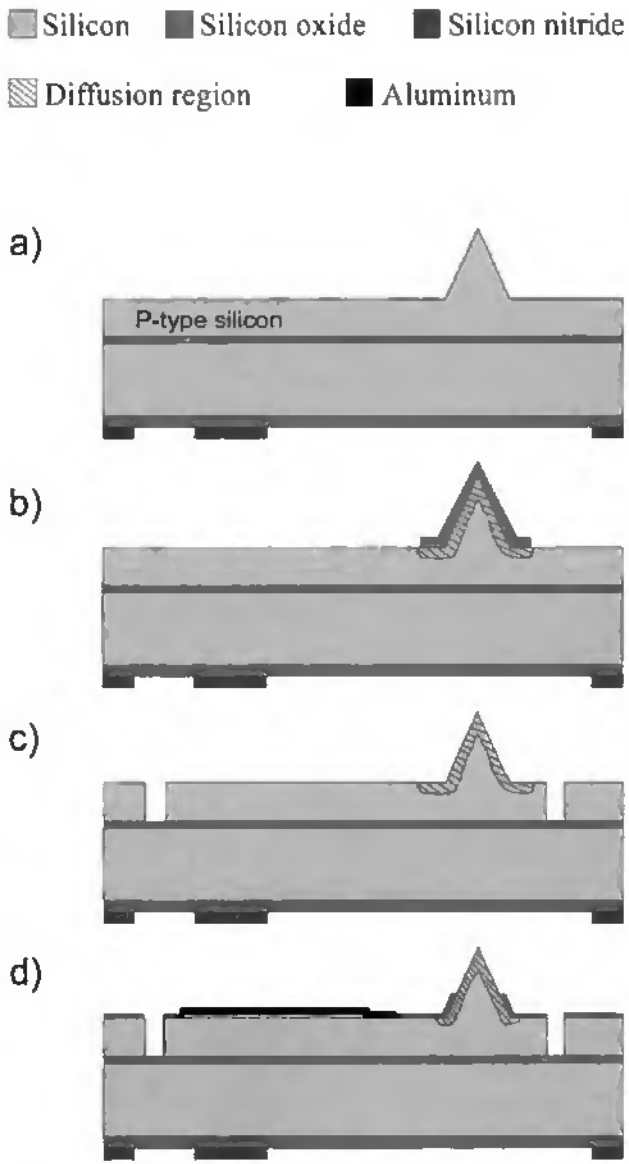
Silicon
Silicon oxide
Silicon nitride
Diffusion region
Aluminum
a)
P-type silicon
b)
c)
d)

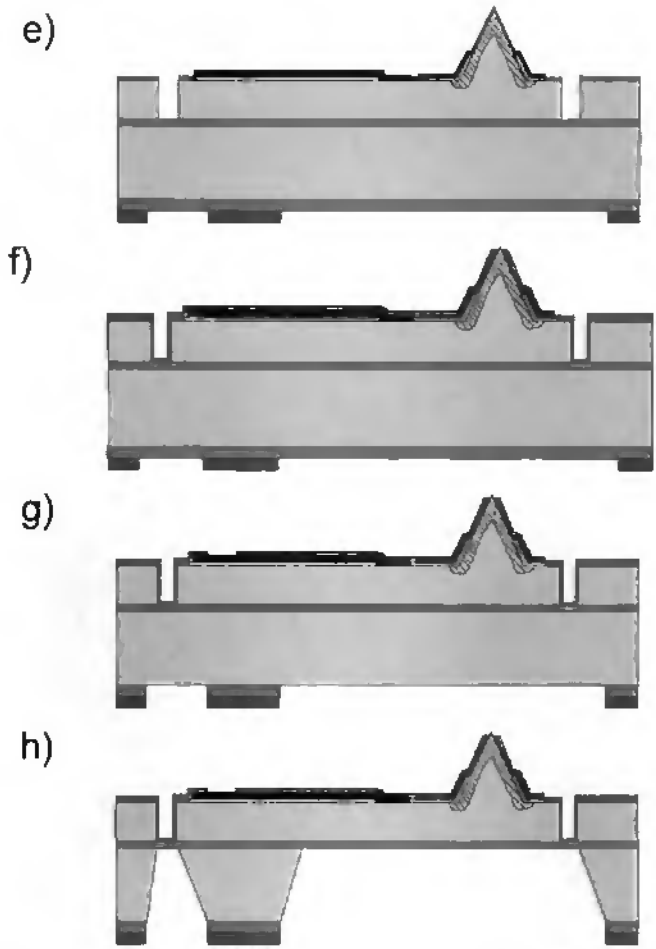

Figure 9.3: Schematic view of the fabrication process. (a) Etching of the tips using KOH (b) Formation of the p-n junction by diffusion (c) Doped oxide removal and dry etching of the cantilevers. (d) Deposition and patterning of the electrodes on an insulating silicon nitride layer. The contact to the p-type substrate is now made (e.f) Aperture fabrication, using a thin aluminum layer and a structured silicon nitride mask.(g) Silicon nitride etching on the contacts pads for the electrodes. (h) Backside etching and releasing of the cantilevers using KOH.

9.2 Fabrication results

Following the previously presented fabrication process probes with different cantilever lengths were fabricated. The mechanical properties are presented in the table below. All cantilevers are 100μm wide and about 5μm thick.

Cantilever length	600 μm	800 μm	1000 μm
Resonance frequency	20 KHz	11 KHz	7 KHz
Spring constant	2.5 N/m	1 N/m	0.5 N/m

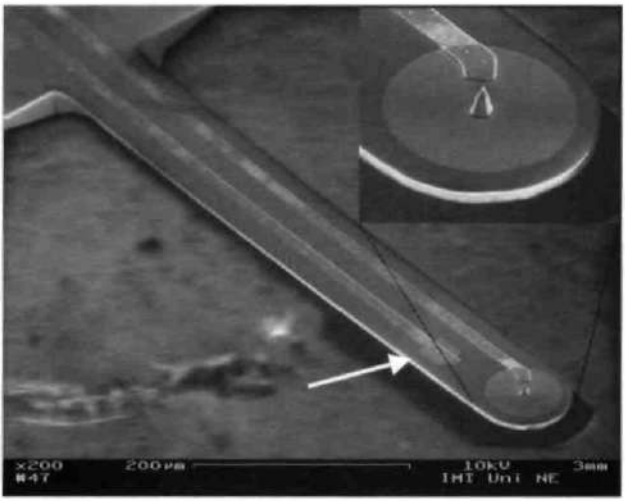

Figure 9.4: SEM micrograph of an 800 μm long cantilever with integrated tip and built in photodiode. The lever is 100μm wide and the silicon tip is 15μm high. The round shape around the tip is the aluminum layer into which the aperture is patterned. The same layer also serves to contact the n-doped tip region. The arrow points at the contact to the p-side of the junction.

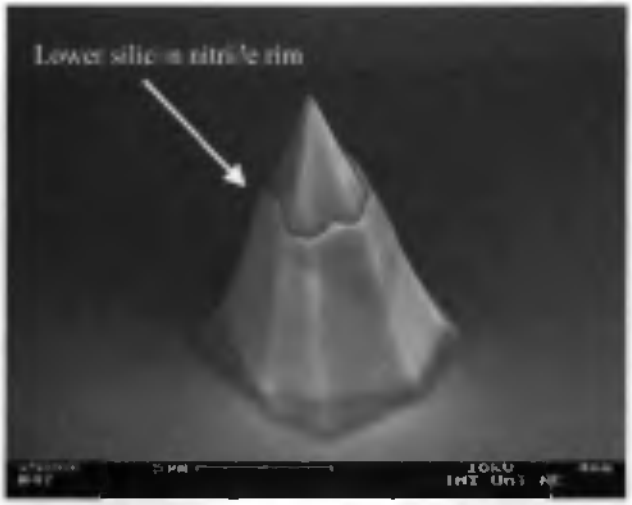

Figure 9.5: Close up view of the measuring tip. The base of the tip is covered with an insulating silicon nitride layer. This silicon nitride layer serves to insulate both regions of the photodiode from each other and is removed on the tip apex to allow contact the n-doped tip region. The whole tip is covered with a 50 nm thin aluminum layer and a 100 nm thick silicon nitride layer used for the aperture formation process. The aperture in the thin aluminum coating at the tip apex cannot be seen on this picture.

9.3 AFM imaging

To test the sharpness of the tips the cantilevers were put into a commercial AFM instrument (© DI Nanoscope III) and dynamic as well as static mode images of a test samples were performed using the standard beam-deflection method.

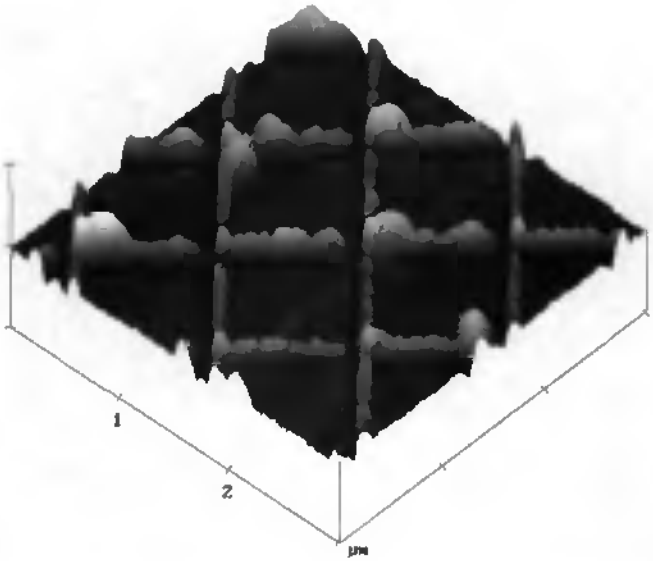

Figure 9.6: AFM image of a 1µm test grid acquired in tapping mode using a 600 µm long cantilevers with integrated p-n junction. The lines are 15nm high.

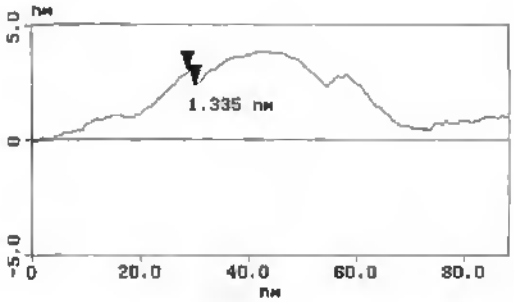

Figure 9.7: High-resolution line-scan using a probe with integrated p-n junction and aperture. The lateral resolution is better than 2nm. This scan was obtained in tapping mode using a commercial AFM setup and the beam deflection method.

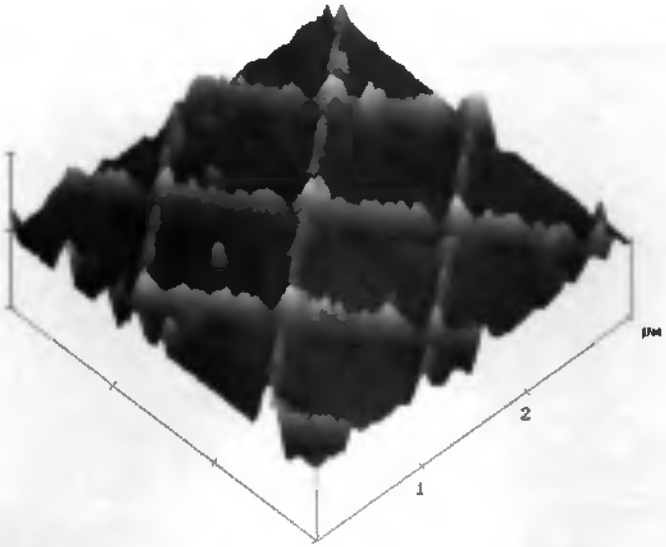

Figure 9.8: AFM image of a 1µm test grid acquired in contact mode using a 1000 µm long cantilevers with integrated p-n junction. The resolution is similar to that obtained in tapping mode.

The AFM resolution obtained using the probes with integrated p-n junction and aperture is not significantly different from the resolution that can be obtained with normal AFM cantilevers. A lateral resolution better than 2 nm was achieved in tapping mode on flat surfaces.

9.4 Electrical properties of the photodiode

The electrical properties of the integrated p-n junction are presented in Figure 9.9. The breakdown voltage of the integrated photodiodes was measured at –13 V. This value is not particularly high because of the high doping concentration of the p-n junction which causes a small depletion zone width. The measured dark current of the diode biased at –6 volts is 1.5 nA.

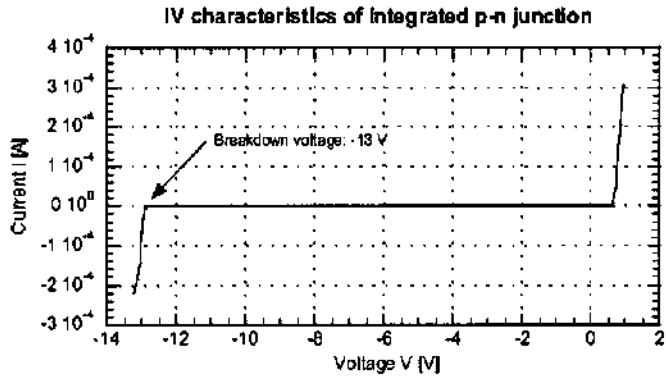

Figure 9.9: typical IV curve of an integrated photodiode.

9.5 Simultaneous AFM and SNOM images

To test the response of the integrated photodiode the probe was scanned over an optically active sample. A laser diode was chosen for this purpose. Again, a commercial AFM instrument (© DI Nanoscope III) was used for imaging. During imaging the photodiode is reverse biased with a DC voltage of 0 V to –5 V. In this configuration the change in current flowing through the junction is proportional to the number of photons reaching the depletion zone. The cantilever deflection is monitored with the standard laser beam deflection method. To minimize the effect of this laser beam on the integrated photodiode signal, the reflection point is displaced along the cantilever away from the tip. During imaging the laser diode was operated below it's lasing threshold. Figure 9.10 shows a simultaneous AFM and SNOM image acquired in contact mode with the diode being biased with a voltage of –5 volts. To reduce noise the laser diode was modulated and the current was measured using lock-in detection. The general elliptic shape of the laser emission is clearly visible.

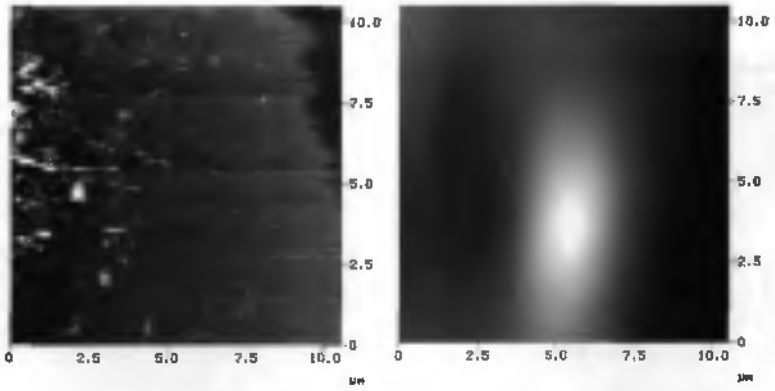

Figure 9.10: Simultaneous AFM and SNOM images of the surface of a laser diode. The left image is the topography and the right image is the photo-current generated inside the integrated p-n junction

Figure 9.11 shows an image of a similar laser diode obtained with a conventional fiber based SNOM microscope. The laser spot is better defined in the fiber-SNOM image than in the image obtained with the integrated photodiode

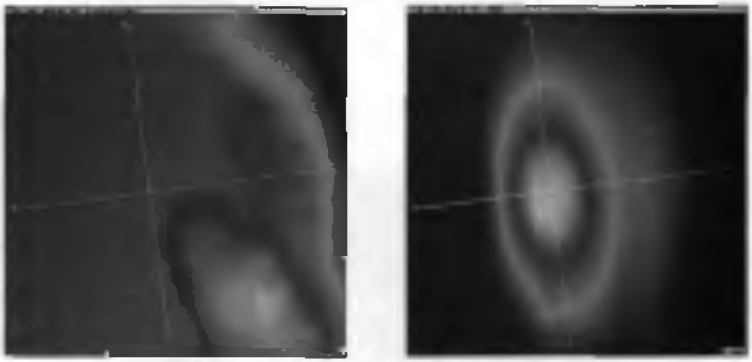

Figure 9.11: SNOM image of a laser diode acquired with a conventional fiber-based microscope. The topography of the laser diode is presented on the left image and the optical image on the right. (Images courtesy H. Heinzelmann).

More precise investigations have shown that the difference between the fiber-based SNOM image and the cantilever-based SNOM image is due to the fact that light can also reach the photodiode through other paths than the aperture. For example, a substantial photocurrent can be generated by locally illuminating the cantilever on the aluminum coating forming the aperture. A current is also measured when the cantilever is illuminated next to this aluminum coating. Thus the image shown in Figure 9.10 is a convolution between different optical contribution.

Several explanations can be given to this behavior. First of all the junction depth at the tip apex is much greater than the junction depth on a flat surface. This is simply due to the fact that during the formation of the p-n junction diffusion occurs from several sides simultaneously. Because of that the photons travelling through the aperture must travel a greater distance in the silicon before reaching the active zone (the depletion zone) of the photodiode. Thus, the tip apex region is particularly insensitive to light. The diffusion process used in the fabrication of the probes generates junctions that are about 1 µm deep on flat surfaces. Figure 9.12 shows that the junction at the tip apex is a least 2 µm deep. This value is too high to achieve a high sensitivity of the tip apex as most of the photons are absorbed before they reach the junction.

This difference in junction depth makes the absence of pinholes in the metal coating and its thickness an important issue because light penetrating the side-walls or the base of the tip can more easily generate a current than light travelling through the aperture. An aluminum coating 50 nm in thickness, as used in the probe fabrication, attenuates the intensity of a light wave only to about 4×10^{-4} of its original intensity. This is not enough compared to the transmission through the aperture, which is in the

same order of magnitude, especially since this contribution is integrated on the whole junction surface.

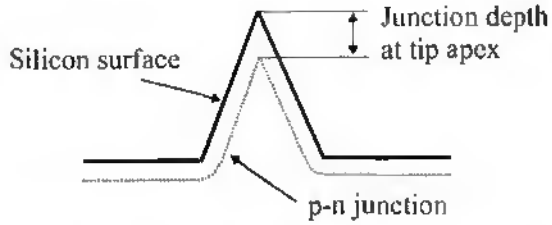

Figure 9.12: Schematic representation of the junction depth formed by diffusion on a silicon tip.

Another possible explanation is the insulating silicon nitride layer located beneath the aluminum coating (Figure 9.3, d and e). This layer could act as a waveguide and bring light from the side of the cantilever to the photodiode.

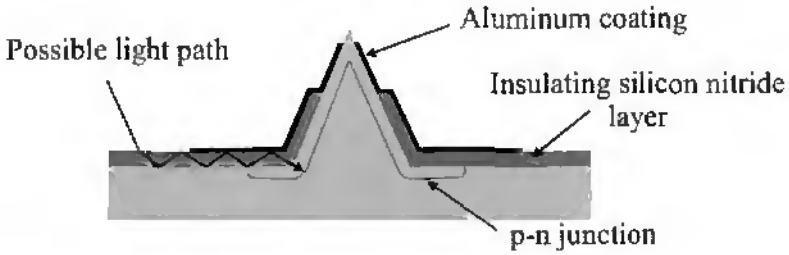

Figure 9.13: Schematic view of the tip region. The silicon nitride layer could guide light to the p-n junction.

The characteristics of the probe can be improved by:

- Reducing the junction depth and increasing the depletion zone width by an optimized doping process. This would render the photodiode more sensitive.
- Increasing the thickness of this aluminum layer to increase the opacity and reduce the number of pinholes on the side of the tip.
- Increasing the size of the aluminum coating into which the aperture is structured so that it totally covers the silicon nitride layer.
- Adding a metal coating to the backside of the cantilever to reduce the effect of the laser used for the beam deflection measurement and further cut down unwanted light reaching the junction.

9.6 Conclusions

The concept for a new type of micromachined nearfield probe with integrated light detector has been demonstrated. Silicon AFM cantilever probes with integrated p-n junctions have successfully been fabricated. Simultaneous AFM and SNOM imaging has been performed. However the present probes need to be optimized in order to increase the sensitivity. At present state they are not well suited for high resolution imaging of radiative samples. It is possible that they can be used for the probing of evanescent fields created by Total Internal Reflection (TIR), but this needs to be verified.

The fabrication process makes it possible to integrate deflection sensors and actuators on the probes, thus opening the possibility for parallel imaging. Also a p-i-n diode or an avalanche diode could be substituted to the p-n junction if a higher sensitivity is necessary.

9.7 References

[1] R. C. Davis ,C. C. Williams and P.Neuzil, *Appl. Phys. Lett.* 66 , (1995), pp. 2309.

[2] S. Heisig, H.-U. Danzebrink, A. Leyk, W. Mertin, S. Münster, E. Oesterschulze, *Ultramicroscopy* 71, 1-4, (1998), pp 99-105.

[3] O. Wolter, Th. Bayer, and J.Greschner, *J. Vac. Sci. Technol. B* 9, 2 (1991), pp. 1353-1357.

[4] S. Roth, L. Dellmann, G-A Racine and N. F. de Rooij, *J. Micromech. Microeng.* 9, (1999), pp. 105-108.

[5] P. F. Indermühle, S. Roth, L. Dellmann and N. F. de Rooji, *J. Micromech. Microeng.* 8, (1998), pp. 74-76.

[6] G. Schürmann, P.F. Indermühle, U. Staufer and N. F. de Rooij, *Surf. Interface anal.* 27, (1999), pp. 299-301.

10 Fabrication of a silicon cantilever probe with transparent quartz tip

This passive probe consists of a silicon AFM cantilever with an integrated amorphous quartz tip. The tip is covered with an aluminum layer with a small aperture at the apex. Below the tip, a hole in the silicon cantilever, allows light to be focused into the backside of the transparent tip (Figure 10.1).

Figure 10.1: Schematic view of the cantilever with an integrated square quartz tip. A hole is machined into the silicon cantilever behind the tip. The nano-aperture at the tip apex is not represented in this diagram.

Quartz is transparent to light from the visible to the ultra-violet range. Therefore it is frequently used in optics. Also, quartz doesn't exhibit any internal fluorescence. However the integration of quartz structures on silicon wafers is very difficult. This arises from the fact that the expansion coefficients of quartz and silicon (0.5×10^{-6} for quartz and 3×10^{-6} for silicon) differ by almost one order of magnitude. For that reason, once a

quartz structure of substantial size and thickness is integrated on the silicon substrate, no process step involving the heating of the wafer to high temperatures can be tolerated anymore. Otherwise, the tensile stress appearing at the interface between the silicon and the quartz can lead to the rupture of the structures. Since many commonly used materials are deposited at temperatures higher than 400°C (silicon nitrides, silicon oxides or polysilicon), the above mentioned condition dramatically limits the choice of materials that can be used during the processing.

10.1 Fabrication sequence

10.1.1 Back-side structuring of the wafers (Figure 10.3, a, b)

For this process 4-inch wafers with a thickness of 520 µm were used. First, silicon oxide is grown on the wafer surface, followed by the deposition of an LPCVD silicon nitride layer, both layers being 200 nm thick (Figure 10.3, a). The nitride and oxide is then patterned on the backside by RIE and wet etching in BHF respectively. The wafer is then etched in KOH until a silicon membrane of about 30 µm in thickness is formed (Figure 10.3, b). The nitride layer on the topside is used to protect the silicon and the oxide layer during this KOH etching.

10.1.2 Cantilever definition (Figure 10.3, c, d)

The now useless silicon nitride on the topside of the wafer is totally removed by dry etching, the silicon surface being protected by the oxide. The oxide on the topside of the wafer is then structured by photolithography and wet etching in BHF (Figure 10.3, c). Using DRIE, the trenches defining the borders of the cantilevers and the holes for the

backside of the tips are etched (Figure 10.3, d). During this 5 µm deep etching the oxide is used as masking material.

10.1.3 Quartz wafer bonding and thinning (Figure 10.3, e, f)

Prior to bonding, the silicon oxide is removed form the top surface by wet etching in BHF (Figure 10.3, e).

At this point of the process a quartz (fused silica) wafer is bonded onto the silicon substrate. Both wafers, silicon and quartz, are cleaned in nitric acid, rinsed in water, dried and brought together. Bonding between the surfaces occurs spontaneously. The bonded wafers are then cured in a vacuum oven at 100°C for 12 hours. This increases the bonding strength. 100°C is the highest temperature at which the silicon-quartz sandwich can be heated without the two wafers seperating again. Good bonding is only possible if both surfaces are perfectly clean and flat. This is the reason why the silicon surface was protected by an oxide layer during the previous steps. The quartz wafer, which is 500 µm thick, is then thinned down to 30 µm in a 50% HF solution (Figure 10.3, f). This takes about 6 hours etching time. During the thinning, the oxide and nitride masks on the backside of the silicon wafer are etched away. Provided the starting surface of the quartz wafer is perfectly clean and smooth, the roughness of the etched down quartz does not significantly increase. A surface roughness of Ra = 15 Å was measured on a thinned down quartz wafer, compared to the starting surface which had a roughness of Ra = 5 Å.

Now that the quartz layer is only 30 µm thick the wafer can be cured at 200°C for further increasing the bonding strength.

10.1.4 Etching of the tips and aperture formation (Figure 10.3, g, h)

The tips are etched into the quartz using a 50% HF acid solution. The masking material is a 500 nm thick amorphous silicon layer. This amorphous silicon is deposited over the quartz at 200°C by a special process [1] and structured with dry etching (Figure 10.3, g). Temperatures of 200°C are now possible since the quartz wafer is only 30 µm thick. The apertures are then structured into an aluminum layer covering the tips (Figure 10.3, h). The metal coating used in this process is a 100nm thick aluminum layer deposited on a 5nm thick titanium adhesion layer. The titanium not only increases the adhesion, it also reduces the surface roughness of the aluminum coating. The following images show three different quartz tips bonded onto silicon cantilevers.

Figure 10.2: SEM images of the quartz tips, bonded on the silicon cantilever. The trenches defining the cantilevers are clearly seen.

10.1.5 Releasing of the cantilevers (Figure 10.3, i)

The last step in the process is to etch away, from the backside, the remaining silicon membrane (Figure 10.3, i). This is done using DRIE. The probes are now attached to the wafer frame by small silicon bridges and can easily be broken out with tweezers.

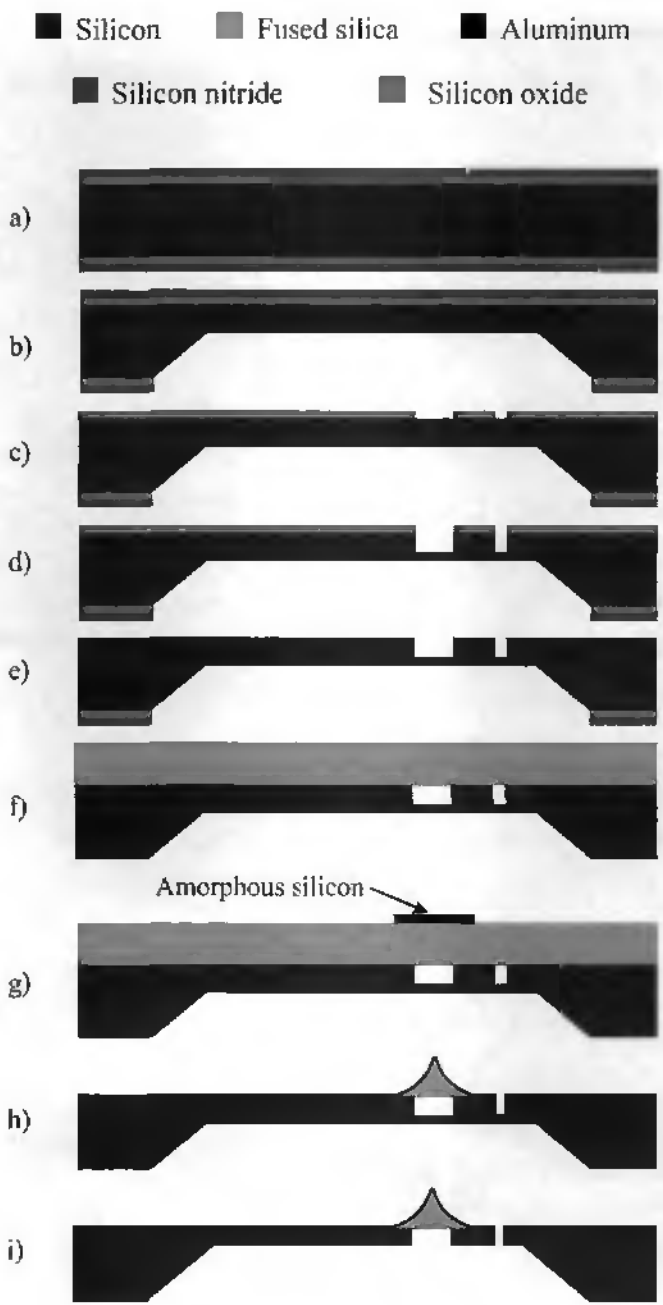
Silicon
Fused silica
Aluminum
Silicon nitride
Silicon oxide
a)
b)
c)
d)
e)
f)
Amorphous silicon
g)
h)
i)

Figure 10.3: Schematic fabrication process of a silicon cantilever with integrated quartz tip. (a) Growth of a silicon oxide and a silicon nitride layer. (b) Backside structuring of the nitride and axide. Partial etching of wafer in KOH. (c) Nitride removal and oxide patterning. (d) Cantilever etching using DRIE. (e) Oxide removal. (f) Bonding and thinning of quartz wafer. (g) Deposition and structuring of an amorphous silicon mask. (h) Etching of tips and aperture formation. (I) Final backside etching using DRIE and releasing of cantilevers.

10.2 Fabrication results

The fabricated cantilevers are 80 µm wide and 5 µm in thickness. They exist in two different lengths depending on their use in static or dynamic mode imaging. The cantilevers for dynamic mode imaging are 400 µm long, have a calculated first mechanical resonance frequency of about 40 kHZ and a spring constant of 7 N/m. The cantilevers for static mode imaging are slightly longer and thus, softer. They are 700 µm in length, have a resonance frequency of 14 kHZ and a spring constant of 1 N/m.

The 25 µm high integrated quartz tips have been fabricated in different shapes. Round, square, and triangular masks have been used for the tip fabrication. The circular tips seem to be the best suited for SNOM imaging as most apertures structured on those tips are round or have only a slight asymmetry. Because of imperfections during the lithography process, a small knife-edge often terminates the square tips. This leads to elongated apertures that could be used for their polarization dependent transmission properties. The triangular tips eliminate the possibility of a knife-edge terminating the tip apex. However their suitability for nearfield imaging has still to be demonstrated.

The holes that are machined into the silicon cantilevers behind the tips are either 10 µm or 20 µm in diameter. This size is sufficient to focus a laser light source into them. The following four images show different finished probes. The slight offset of the tips with respect to the cantilever is due to a bad alignment during the lithography defining the tip etching pads.

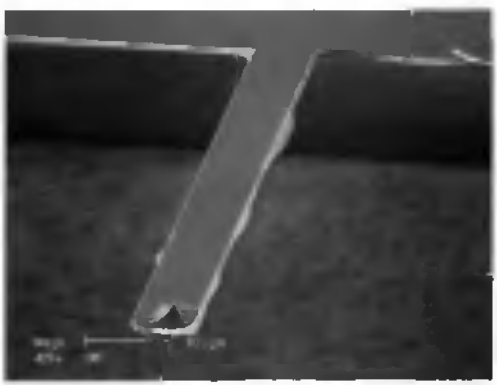

Figure 10.4: SEM photograph of a 700 µm long cantilever with square quartz tip. The whole cantilever is still covered with a thin layer of quartz.

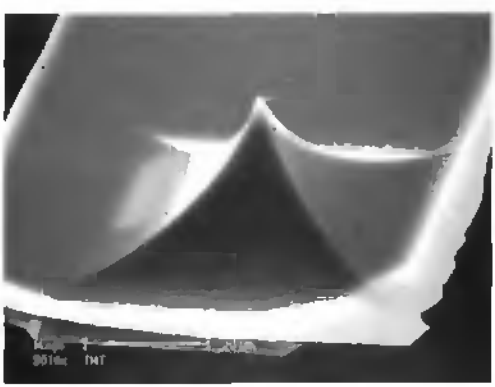

Figure 10.5: Detailed view of the SNOM tip.

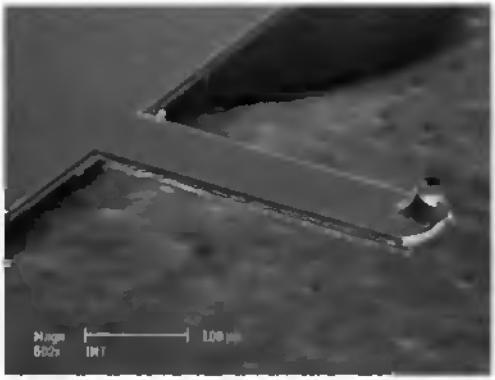

Figure 10.6: SEM picture of a 400 µm long silicon cantilever with integrated circular quartz tip. A thin layer of quartz still covers the cantilever.

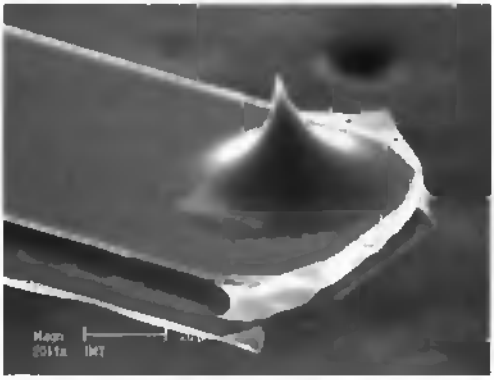

Figure 10.7: Detailed view of the round tip.

10.3 Probe characterization

To test the suitability of the probes for AFM imaging, images in static and dynamic mode of a 1 µm test grid were acquired using a commercial instrument (© Nanoscope III). The images show a good resolution comparable to that obtained with commercial AFM tips. The static mode

image was obtained using a 700 μm long cantilever probe whereas the dynamic mode image was obtained with a 400 μm long cantilever. Both cantilevers had an integrated round quartz tip.

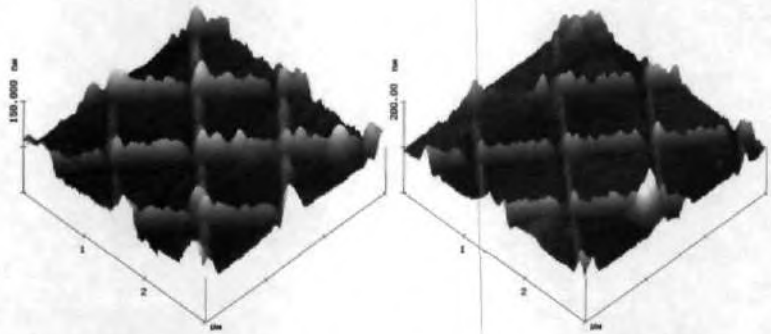

Figure 10.8: AFM images of a 1 μm test grid obtained with the cantilevers with integrated quartz aperture tip, in static (left image) and dynamic mode imaging (right image).

The presence of an aperture at the tip apex was verified by focusing a laser beam into the backside of the tip and by observing the light emitted by the tip apex. Figure 10.9 shows a top view of the extremity of a cantilever with integrated square quartz tip. The cantilever is illuminated from the back with a laser beam. It can be seen that the tip is covered with a pinhole-free metal coating and that an aperture is present at the tip apex. The stray light around the cantilever comes from reflections inside the optical system.

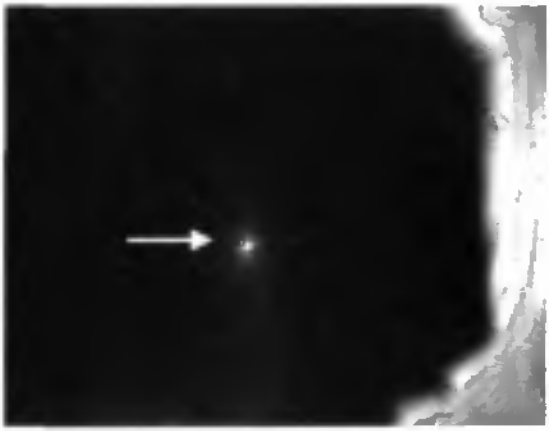

Figure 10.9: Image of the light transmitted through a quartz tip integrated on a silicon cantilever. The arrow points to the light emitted from the aperture. The stray light in the background comes from reflections in the optical system (courtesy M. Freyland).

10.4 Simultaneous AFM and SNOM imaging

Using the cantilevers with integrated quartz tips, simultaneous AFM and SNOM imaging in illumination mode was performed. The images were acquired using a specially designed mounting head. This head allows two laser beams to be focused onto the backside of the cantilever. The first beam is focused onto the quartz tip and its position is adjusted until light is transmitted through the aperture at the tip apex. The other beam is used for monitoring the deflection of the cantilever. Its reflection point is slightly displaced along the cantilever away from the tip, towards the bulk of the chip.

Two different samples were imaged. The first sample consists of a grid of 1.5 μm wide and 70 nm thick, opaque, aluminum lines on a transparent pyrex-glass substrate. The second sample is a metal pattern obtained by using closely packed 200 nm in diameter latex spheres as shadow masks during metal evaporation. This results in a hexagonal array of small metal islands, the mean distance between two adjacent islands being about 115 nm.

Figure 10.10 shows a simultaneous SNOM and AFM image obtained from the aluminum lines sample. The images were recorded in contact mode.

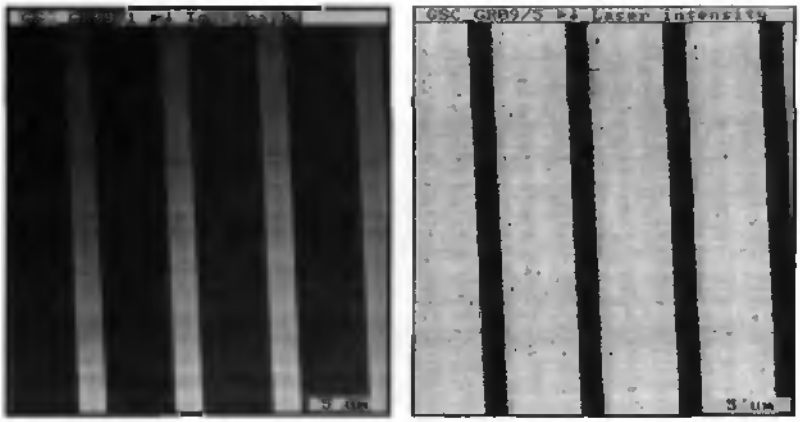

Figure 10.10: Simultaneous AFM and SNOM imaging of a grid consisting of 1.5μm wide and 70 nm thick aluminum lines on a pyrex substrate. The left image is the topography recorded in contact mode and the right image is the detected light intensity.

Figure 10.11 shows an image of the latex sphere projection pattern. This image was obtained by increasing the tip to sample distance and by turning off the topography feedback. This was done in order to reduce the influence of topography as much as possible [2]. The small metal islands are clearly resolved. Therefore, since they are 115 nm apart, the resolution obtained with this probe is considerably better than 100nm.

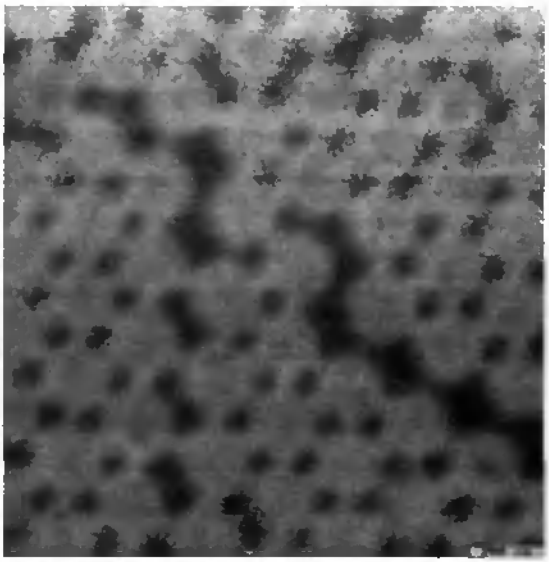

Figure 10.11: SNOM image of a latex sphere projection pattern. The mean distance between two adjacent metal islands is 115 nm.

These images were realized by R. Eckert, as part of his thesis work.

10.5 Conclusion

Combined SFM and SNOM probes have been fabricated. They consist of a silicon cantilever with an integrated 25 µm high quartz tip. Behind the quartz tip a hole in the cantilever allows access to the backside of the tips. The probes are suited for dynamic as well as static mode AFM imaging. Simultaneous SNOM imaging in illumination mode and AFM imaging in contact mode was demonstrated. SNOM images of a sample constituted by small metal islands 115 nm apart have been obtained. From these images one can conclude that the optical resolution of the probes is considerably better than 100 nm.

The deflection of the cantilever can be measured with the beam deflection method. However the laser source needed for this kind of detection scheme produces some background signal. To eliminate this noise source it should be possible to integrate a deflection sensor such as a piezoresistor on the cantilever.

10.6 References

[1] U. Kroll, D. Fischer, J. Meier, L. Sansonnens, A. Howling, A. Shah, "Fast Deposition of a-Si:H Layers and Solar Cells in a Large-Area (40x40 cm2) VHF-GD Reactor", *Mat. Res. Soc. Symp. Proc.* Vol. 557 (1999), pp.121-126.

[2] B. Hecht, H. Bielefeldt, Y. Inouye, D. W. Pohl, L. Novotny, *J. Appl. Phys.* 81, 6 (1997), pp. 2492-2498.

11 Final conclusions and outlook

The widespread use of Scanning Nearfield Optical Microscopy is impeded by the fact that the existing microscopes are difficult to use and produce inconsistent results. This is mainly due to the quality of the SNOM probes themselves. Compared to Atomic Force Microscopy no "standard" SNOM probes, with well-defined properties, exist.

In this thesis micromachining techniques were used for the development of new SNOM probes. The use of micromachining for the fabrication of these probes has different advantages:

- The SNOM tip can be integrated on an AFM cantilever. By doing this the distance regulation is simplified and the probes are rendered less fragile. Furthermore, deflection sensors and actuators can be integrated on the cantilevers, thus, further simplifying the measuring setup and opening the possibility for parallel imaging.
- A better homogeneity in probe characteristics can be achieved by using well-established microfabrication techniques.
- The probes can be batch-fabricated in great numbers. Therefore the price for a high quality probe could be lowered.

Two different SNOM probes were microfabricated: an "active" probe and a "passive" probe.

The "active" probe consists of a silicon AFM cantilever with an integrated tip. A photosensitive p-n junction is integrated into the tip, which is

covered with an opaque aluminum layer into which a nanometer-sized aperture is machined at the apex. Using this probe simultaneous AFM and SNOM imaging was demonstrated. However the probe needs to be optimized in order to achieve a higher optical resolution and sensitivity. An advantage of this probe is that no collection optics are needed. Thus, by adding a sample illumination unit, standard AFM instruments can also be used for SNOM imaging. Furthermore, by integrating deflection sensors and actuators on each cantilever, arrays of such probes could be used for parallel imaging.

The "passive" probe consists of a thin silicon cantilever with an integrated quartz tip. Again, the tip is covered with an opaque aluminum layer with a nano-aperture at the apex. An opening in the cantilever allows light to be detected or focused into the tip from the backside. In comparison to the "active" probe, which can only measure the local optical intensity of a sample, this probe can benefit from all optical contrast mechanisms. These probes were used for simultaneous AFM and SNOM imaging and an optical resolution better than 100 nm was obtained.

To allow the fabrication of these probes, a new nano-structuring technique, relying on a tip effect during RIE was developed. Using this method, SNOM apertures down to 30 nm in diameter were patterned on different microfabricated tips. These apertures were then characterized optically and by SEM observation. This versatile batch-structuring method is insensitive to tip height and fully CMOS compatible. Therefore it can easily be integrated into an existing microfabrication process. Nano-cavities and nano-electrodes were also fabricated using the same technique.

The use of the probe with integrated p-n junction has shown that stray-light generated signal is an important issue. Therefore, during the design of an "active" probe, careful consideration must be given to the following aspects. To avoid stray-light from reaching the aperture, the probe should be fully encapsulated in a thick opaque metal layer. This includes the front and the backside of the AFM cantilever. An aluminum layer, 50 nm in thickness, is not opaque enough. Also, the photosensitive element should be small in size and located close to the tip apex.

The optical characterization of apertures structured on quartz tips has shown that qualitative information about the shape of an aperture can be gained by observing the emission pattern of the aperture in the far-field. By numerically calculating the patterns produced by non-round apertures such as square, triangular, or elongated apertures one could further improve this characterization method.

Finally, the fabrication process of the "passive probe" proves that quartz structures, of substantial size, can be integrated on a silicon substrate. Therefore, new interesting devices can be fabricated. The SNOM cantilever probe with integrated quartz tip is one example. These probes show a great potential for SNOM imaging.

The Integrated Circuits (IC) industry is constantly decreasing the size of electric components. To fabricate such small structures special lithography techniques have been developed such as E-beam lithography, deep-UV lithography, or X-ray lithography. All these techniques are very expensive and technologically demanding.

A real alternative to these methods would be using SNOM probes for high-resolution optical lithography. However, in order to increase the throughput large arrays of probes must be used. Figure 11-1 shows an array of quartz tips with nano-apertures that could be used for this

purpose. Such arrays could also be used in high-density optical data storage.

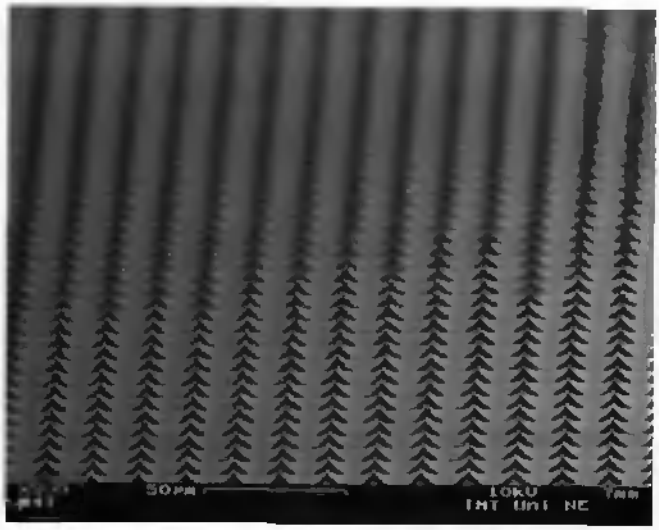

Figure 11-1: Array of quartz SNOM tips for high-resolution near-field lithography.

Acknowledgments

First of all I would like to thank Prof. N. F. de Rooij for giving me the great opportunity to work in his research group. Thank you for trusting me and supporting me during these four years. I must say that the time I spent here at the IMT was most enjoyable. It was a privilege to be part of this extremely stimulating and multidisciplinary working environment.

I want to take this opportunity to thank all the past and present members of samlab which have directly or indirectly contributed to the success of this work, with their numerous, advice, discussions and by creating a pleasant atmosphere.

In particular I am very grateful to Dr. U. Staufer for supervising me, correcting this thesis and helping me in many ways during this work. It was a real pleasure to work with somebody who has such a sense of humor. Dr. Wilfried Noell also contributed to this work with his extensive knowledge of the SNOM world. I am grateful to him for his generosity and willingness to help.

Dr. P. F. Indermühle introduced me to the SPM world and the IMT clean-room. His precious advices at the beginning of the project were highly appreciated. I also want to thank him for his generosity and sense of humor, which he showed by organizing mountain trips, lending us a part of his carpet in Davis CA, supporting us morally from the top of Chaumont and participating in some KTS activities.

I have to express my deepest thanks to the technical staff namely: Sylvain Jeanneret, Pierre-Andre Clerc, Sylviane Pochon, Sabina Jenny, Gianni Mondin, Bastien Droz and José Vaquera. This work would not have been possible without their excellent collaboration. In particular, I want to thank P. A. Clerc for his efficiency and flexibility in the lab and his many

discussions about the magic of snowboarding. Also, I express my gratitude to Signore Gianni Mondin for his ever-cool attitude and his maximum flexibility at handling any kind of exotic processing steps. Thank you Sylviane Pochon for dicing wafers, doing wire bondings, encapsulating various chips and organizing outdoor activities.

I also want to thank Pr. H. P. Herzig, Dr. H. Heinzelmann (CSEM), Pr. A. J. Meixner (Siegen D) for accepting to be co-examiners of this thesis.

Our scientific partners in this project, Dr. Moritz Freyland and Rolf Eckert from the CSEM also contributed to this work. Thank you Rolf for doing the wonderful SNOM measurements using the probes with integrated quartz tips.

At the beginning of this project I spent a lot of time in the chemical lab trying to unravel the secrets of electropolymerization and electrocoagulation. I am grateful to Pr. Milena Koudelka-Hep, Pr. H. Siegenthaler (Uni BE) and Dr. Peter van der Wal for helping me during these unfortunately unsuccessful experiments.

Special thanks go to Dr. Peter Torres and Dr. Ulrich Kroll for kindly providing me with essential amorphous silicon layers.

I also want to thank Dr. Cynthia Beuret for her helpful suggestions on how to manage "surprises" during critical process steps and for shearing her knowledge of KOH etching.

I am also grateful to Dr. Terunobu Akiyama for helping during some AFM and SNOM measurements and lending his special amplifiers.

Thank you Gian-Luca Lettieri for your enthusiasm during your semester work.

Many thanks go to Dr. M.G.H. Meijerink for lending me his name for the tour du canton and being available for various other outdoor activities such as hiking, skiing, picnicking, and the famous Fête des Vendanges.

Thank you Dr. Philippe Luginbuhl for refreshing my Russian vocabulary and thank you Dr. Camille Stebler for shearing the office and offering a place to sleep in California.

Thank you Mr "Coolman" alias Benny Guldimann for showing me the real values in life: working, sports (fitness), snowboarding and beach-volley to mention a few only. Thank you Philippe Dubois for reviving my passion for skiing and rock-climbing.

I am equally grateful to Mr. Danick Briand for making the end of my stay in Neuchâtel more pleasant.

I wouldn't like to end this chapter without expressing my deepest gratitude to the co-founders, past and present members, of the famous non-profit organization KTS, namely S. Roth, L. Dellmann, Dr. PFI and "Baston la menace". It was a great honor to be part of this extremely creative organization which activities were focused on organizing various social events.

List of pubilcations

P.-F. Indermühle, G. Schürmann, G.-A. Racine, N. F. de Rooij, Self-sharpening tip integrated on micro cantilevers with self-exciting piezoelectric sensor for parallel atomic force microscopy, *Appl. Phys. Lett.* 70, 17 (1997), pp. 2318-2320.

P.-F. Indermühle, G. Schürmann, G.-A. Racine, N. F. de Rooij, Fabrication and characterization of cantilevers with integrated sharp tips and piezoelectric elements for actuation and detection for parallel AFM. *Sensors and Actuators* A 60, (1997), pp. 186-190.

P.-F. Indermühle, G. Schürmann, G.-A. Racine, N. F. de Rooij, Atomic force microscopy using cantilevers with integrated tips and piezoelectric layers for actuation and detection, *Journal of Micromechanics and Microengineering* 7, (1997), pp. 218-220.

G. Schürmann, P. F. Indermühle, U. Staufer, N. F. de Rooij, Micromachined SPM probes with sub-100 nm features at tip apex, *Surface and Interface Analysis* 27, (1999), pp. 299-301.

H. Heinzelmann, J.M. Freyland, R. Eckert, Th. Huser, G. Schürmann, W. Noell, U. Staufer, N. F. de Rooij, Towards better scanning near-field optical microscopy probes - progress and new developments, *Journal of Microscopy* 194, 2 (1999), pp. 365-368.

G. Schürmann, W. Noell, U. Staufer, N. F. de Rooij, Microfabrication of a combined AFM-SNOM sensor, *Ultramicroscopy* 82, (2000), pp.33-37.

Conferences and proceedings

P.-F. Indermühle, G. Schürmann, G.-A. Racine, N. F. de Rooij, Fabrication and characterization of cantilevers with integrated sharp tips and piezoelectric elements for actuation and detection for parallel AFM applications, proceedings of Eurosensors X, Leuven, Belgium, September 1996, pp. 481-484.

P.-F. Indermuhle, G. Schürmann, G.-A. Racine, N. F. de Rooij, Tip integration on arrays of silicon micro cantilevers with self exciting piezoelectric sensor for parallel AFM applications, Digest of technical papers of the 9th Internat. Conf. on Solid-State sensors & actuators, TRANSDUCERS '97, Chicago, USA, Vol. 1, pp. 451-453, 1997.

G. Schürmann, W. Noell, U.Staufer, N. F. de Rooij, Microfabricated, light-sensitive AFM probe for scanning near field optical microscopy, Digest of Technical Papers 10th Internat. Conf. on Solid-State sensors and actuators, TRANSDUCERS '99, Sendai, J, vol. 1, pp. 614-617, 1999.

G. Schürmann, P.-F. Indermühle, G. A. Racine, and N. F. de Rooij, Microcantilevers with integrated tip and integrated piezoelectric layers used for actuation and detection in AFM imaging, Poster presented at Nano Hasliberg 2, 2nd Hasliberg workshop on nanoscience (1996), p70.

G. Schürmann, U. Staufer, P.-F. Indermühle, H. Heinzelmann, and N. F. de Rooij, Micromachined SPM probes with sub 100 nm features at tip apex, Poster presented at Nano Hasliberg 3, 3nd Hasliberg workshop on nanoscience (1998), p65.